JOURNAL OF Applied Polymer SCIENCE

Temperature dependent dielectric properties of self-standing and flexible poly(vinylidene fluoride) films infused with Er^{3+} doped GeO_2 and SiO_2 nanoparticles

Epsita Kar,[1] Navonil Bose,[1] Sukhen Das,[1] Nillohit Mukherjee,[2] Sampad Mukherjee[1]

[1]Department of Physics, Indian Institute of Engineering Science and Technology, Howrah, India

[2]Centre of Excellence for Green Energy and Sensor Systems, Indian Institute of Engineering Science and Technology, Howrah, India

Correspondence to: S. Mukherjee (E-mail: smukherjee.besu@gmail.com)

ABSTRACT: The synthesis of Er^{3+}@GeO_2 and Er^{3+}@SiO_2 nanoparticle impregnated self-standing poly(vinylidene fluoride) films by a facile solution casting technique has been reported. The prepared films were thoroughly characterized using X-ray diffraction technique, field emission scanning electron microscopy, and transmission electron microscopy. The optical properties were evaluated using UV–Vis spectroscopy. Detailed study on the temperature dependent dielectric properties of the composite films with different Er^{3+} content were also investigated to establish the electrical properties of the same, which revealed the presence of different relaxation processes, namely, α_c and ρ. Due to the smaller size, Er^{3+}@SiO_2 was found to disperse better in the PVDF matrix than Er^{3+}@GeO_2, which resulted in higher dielectric constant of the former at 300 K. At higher temperature (403 K), the behavior was reversed due to the formation of larger sized low mobility complexes. An investigation on ac conductivity proved the conduction mechanism for neat as well as composite PVDF films to follow the Correlated Barrier Hopping model. The loading of Er^{3+}@GeO_2 and Er^{3+}@SiO_2 nanoparticles in the PVDF matrix significantly enhances the dielectric properties without losing the flexibility of the composite films. © 2016 Wiley Periodicals, Inc. J. Appl. Polym. Sci. **2016**, *133*, 44016.

KEYWORDS: characterization; dielectric properties; nanoparticles; nanowires and nanocrystals; properties

Received 3 December 2015; accepted 2 June 2016

DOI: 10.1002/app.44016

INTRODUCTION

Polymer nanocomposites, a new class of material has earned tremendous popularity among the scientists and technologists due to their unique electrical, thermal, and mechanical properties.[1] The improved properties of nanocomposites may be attributed to the addition and dispersion of highly anisotropic nanofillers.[2] Since the size of fillers are in nano-dimension, the interfacial interactions between the nanofillers and polymer matrix increase significantly due to the high surface-to-volume ratio of the nanofillers, which results in improved physicochemical properties of the polymer. Hence, addition of small amount of nanofillers is sufficient to improve the polymer properties without significantly compromising the polymer flexibility, optical transparency, and other properties in comparison to neat polymer. Among the polymer nanocomposites, poly(vinylidene fluoride) (PVDF) nanocomposites have attracted much attention due to their potential use in high energy-density capacitors, electrostriction for artificial muscles, magnetostriction for nanoparticles, and smart skins for drag reduction.[3–7] In addition to that PVDF has its wide applications in biotechnology,[8] photorecording,[9] and rechargeable lithium batteries.[10] Recently the oxides of group IV materials, namely, SiO_2 and GeO_2 are gaining paramount importance due to their contribution to obtain efficient dielectric properties without sacrificing the flexibility of the polymer nanocomposites. In this context, it is worthwhile to mention that, several works have been done using PbS[11] and SiO_2[12] as nanofillers in PVDF to enhance the electrical properties. More over SiO_2 and GeO_2 nanoparticles can be used as nanofillers for PVDF matrix due their abundance, low cost, and green additive nature.

PVDF ([—CH_2—CF_2—]) is a semicrystalline polymer exhibits five different crystalline phases α, β, γ, δ, and ε.[13] Out of these phases, the α is the non-polar form of PVDF which is the most thermodynamically stable state at ambient temperature and

This article was published online on 26 Jun 2016. An error was subsequently identified in the graphic to Figure 2. This notice is included in the online and print versions to indicate that both have been corrected 07 July 2016.

pressure. Most usually this α phase occurs with a dominating fraction in the melt processed PVDF film. However, the β and γ phases are the polar phases of PVDF, where β phase assumes paramount importance over the other phases due to its better piezoelectric, ferroelectric, and pyro-electric properties.[14,15] The α phase PVDF possess TGTG′ (T-trans, G-gauche$^+$, G′-gauche$^-$), β phase has all trans (TTT) and the γ phase has 3TG3TG′ conformations.[13,16] As a consequence, different techniques including incorporation of different fillers have been developed to enhance the β phase content in PVDF. Recently, our group has shown that by adding SiO_2 and GeO_2 nanoparticles, a notable transformation of PVDF from α phase to β phase can be achieved with significant enhancement in dielectric and other electrical properties.[17]

Rare earth (R^{3+}) ions possess some unique features like special chemical characteristics, including a relatively large size, low capacity for covalent bond formation, and electrostatic interaction with negatively charged ligands. This favors in an electronic structure which results in ionic complex formation.[18,19] These rare earth complexes have their wide applications in light emitting diodes, optical fibers, laser materials, and optical signal amplifiers. In addition, these rare earth materials have significant effects on the physicochemical properties of polymers[20–23] due to their capability of interaction with the polymer chain. As a consequence, rare earth materials/ions doped PVDF composites are being studied recently,[24,25] where dielectric properties of erbium chloride, gadolinium chloride,[24] and lanthanum chloride[25] loaded PVDF matrix have been studied extensively.

Study on dielectric properties and related relaxation processes of ferroelectric polymers like PVDF and its composite films[24–27] have received great interest from the last decades. The objective of our work is to have enhanced dielectric properties using relatively small amount of rare-earth material, which will bring cost-effectiveness. On the other hand, the use of GeO_2 and SiO_2 nanoparticles as the primary host of erbium ions in the polymer matrix will also be of interest to study due to their unique electronic interactions. The analysis of the effect of rare-earth ions without any anionic part will also have a significant role in this present work.

EXPERIMENTAL

Materials

PVDF pallets with average molecular weight M_w: 275,000 g/mol (M_n: 107,000) were obtained from Sigma Aldrich, The United States. Erbium nitrate pentahydrate ($Er(NO_3)_3$, $5H_2O$) (M_w: 443.35 g/mol, 99.9%) was obtained from Sigma Aldrich, the United States. Dry N,N-dimethyl formamide (DMF, Mecrk, India), germanium oxide (Alfa Aesar, 99.9%), tetraethyl orthosilicate (TEOS, Mecrk, Germany), ethanol (Merck, Germany), and ammonia (strength 30%) were used in this work. All the materials were used without further purification.

Synthesis of GeO_2 and SiO_2 Nanoparticles

GeO_2 nanoparticles (NPs) were synthesized using typical hydrothermal method[28] taking GeO_2 powder as the starting material. The details of synthesis of GeO_2 nanoparticles were given elsewhere.[20] The nanoparticles were synthesized at a temperature of 185 °C and the product was collected by evaporation of excess water.

The SiO_2NPs were synthesized by the modified Stöber's method.[29] In this typical preparation technique, initially a mixture of 160 mL ethanol, 40 mL distilled water, and 5 mL of ammonia was prepared by vigorous stirring for 30 min. Then 2 mL of TEOS was slowly added into the resulting mixture which was stirred for 12 h by using a magnetic stirrer at room temperature (30 °C). Finally, the resulting solution was dried to obtain SiO_2 NPs.

Synthesis of Erbium Doped GeO_2 and SiO_2 Nanoparticles

In order to incorporate erbium (Er^{3+}) ions into the synthesized GeO_2 and SiO_2 nanoparticles, the oxides were immersed into $Er(NO_3)_3$, $5H_2O$ solution of different strengths (0.02, 0.05, and 0.1*M*). The solution was kept for 24 h followed by an annealing process at a temperature of 250 °C for 2 h. Then the product was collected and washed by distilled water for several times for the complete removal of residual $Er(NO_3)_3$.

Synthesis of Er^{3+}@GeO_2 and Er^{3+}@SiO_2 Loaded PVDF Films

The PVDF composite films impregnated with Er^{3+}@GeO_2 and Er^{3+}@SiO_2 were synthesized by the simple solution-casting method. In a typical synthesis procedure, 500 mg of PVDF was dissolved in 10 mL DMF at 60 °C by stirring until complete dissolution of PVDF in DMF was achieved. Then a particular amount (15 wt %) of both type of fillers (containing different molar concentration of erbium) were added in the solution of PVDF and the resultant mixture was vigorously stirred for 12 h followed by 30 min of sonication to obtain a homogenous solution. The composite films were obtained by casting the whole mixture in a properly cleaned and dried Petri dish and evaporating the solvent at 90 °C in a hot air oven. Neat PVDF films were also prepared following the same procedure to carry out the comparative study. The thicknesses of the as synthesized neat PVDF and composite films, were nearly about 80 ± 2 μm as determined by thickness profiler (Bruker DEKTAK XT). The schematic of the synthesis procedure is shown in Figure 1 and the detail composition of the synthesized samples is given in the Table I where Er^{3+}@GeO_2/PVDF composite films are named as PGE and Er^{3+}@SiO_2/PVDF composite films are as PSE.

Characterizations

The structural properties of the as synthesized films were studied by using X-ray diffractometer (Bruker-D8) with Cu-Kα radiation (λ = 1.541 Å) using Bragg–Brentano goniometer geometry and θ–2θ scanning mechanism. To study the morphology of the PVDF nanocomposite films, field emission scanning electron microscopy (FESEM) (INSPECT F50, Netherlands) was used. The Energy dispersive X-ray spectroscopy (EDS) of the samples was performed by Bruker attachment with FESEM. To have a detail idea about the structural properties of the polymer/nanoparticles composites, transmission electron microscopy (TEM, TECNEI G2) was used. The dielectric properties of the PVDF nanocomposite films were studied using a digital LCR meter (Agilent, E4980A). The value of the dielectric constant (ε′), tan δ, dielectric loss and total ac conductivity (σ_{ac}) of the samples are calculated using the following equations,[17]

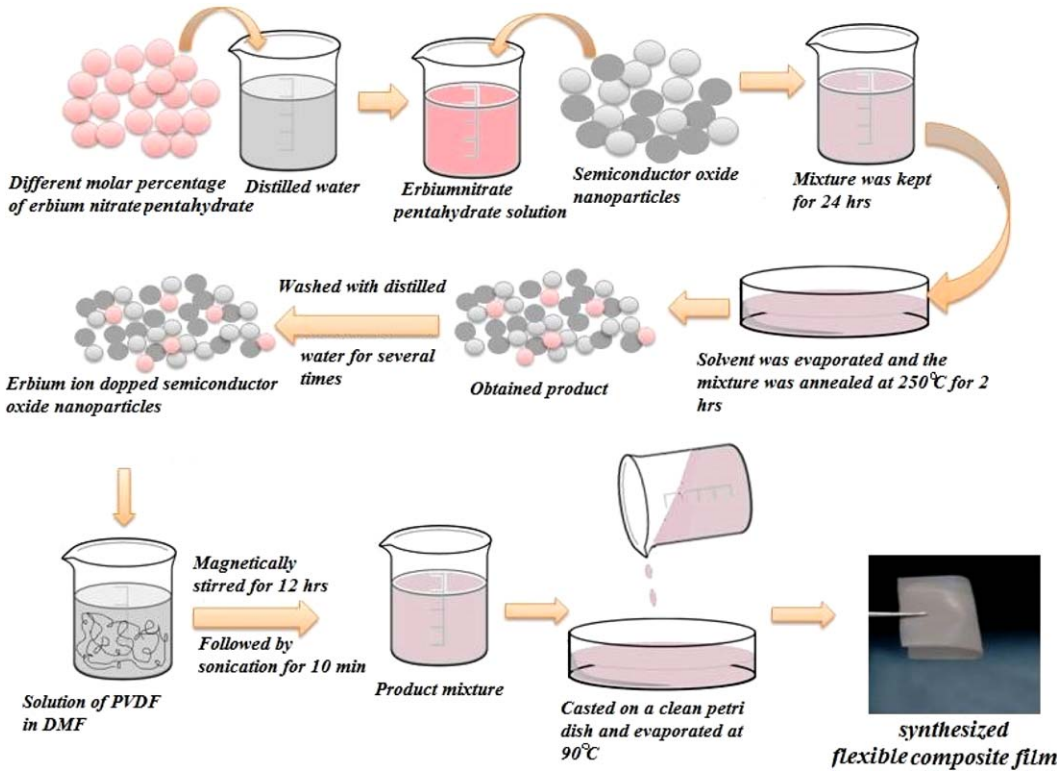

Figure 1. Schematic diagram of the synthesis procedure of the as synthesized Er^{3+}@GeO_2 and Er^{3+}@SiO_2 loaded PVDF films. [Color figure can be viewed in the online issue, which is available at wileyonlinelibrary.com.]

$$\varepsilon' = \frac{C \cdot d}{\varepsilon_0 A} \tag{1}$$

and

$$\tan\delta = \frac{\varepsilon''}{\varepsilon'} \tag{2}$$

$$\text{that is } \varepsilon'' = \tan\delta \times \varepsilon'$$

$$\sigma_{ac} = i\omega\varepsilon_0\varepsilon'' \text{ where } \omega = 2\pi f \tag{3}$$

where, C, d, A, tan δ, and ε'' are the capacitance, thickness, effective area, tangent loss, and dielectric loss of the samples, respectively. f is the frequency of the electric field applied across the samples and ε_0 is the free space permittivity (8.854×10^{-12} F/m). These electrical measurements were carried out using silver electrodes (having area 1 cm × 1 cm), in the frequency range 100 Hz to 1 MHz and within the temperature range 300–403 K.

From the study of various electrical parameters, it has been found that, best electrical and optical properties were exhibited by 0.1% Er^{3+}@GeO_2 and 0.1% Er^{3+}@SiO_2 in PVDF films. So, in order to avoid data redundancy, here, we have provided the structural analyses of 0.1% infused materials.

RESULTS AND DISCUSSION

X-ray Diffraction Analysis

Figure 2(a–c) shows the XRD patterns of samples P0, PGE0.1 and PSE0.1, respectively. The XRD pattern of neat PVDF (P0) reveals peaks around the 2θ values of 17.8°, 18.5°, 20°, and 26.7° corresponding to the (100), (020), (110), [(201),(310)] planes of α phase PVDF, respectively.[30] Another peak positioned at 38.7° may be attributed to the (211) plane of the γ phase of PVDF.[17] In Figure 2(b), a well recognizable peak positioned at 2θ = 26.2° is clearly indexed to the (101) plane of cubic crystalline phase of GeO_2 (JCPDS File No.−43-1016), this infers the incorporation of GeO_2 nanoparticles in the PVDF matrix. The broad peak positioned around 2θ = 20° for PGE0.1 is occurred due to the presence of both α and β phases of PVDF [(110),

Table I. Details of the Composition of the as Synthesized PVDF Composite Films

Name of the sample	Type of the semiconductor oxides	Strength of the added erbium nitrate pentahydrate [$Er(NO_3)_3$, $5H_2O$] solution (molar %)
P0	—	0
PGE0.02	GeO_2 nanoparticles	0.02
PGE0.05		0.05
PGE0.1		0.1
PSE0.02		0.02
PSE0.05	SiO_2 nanoparticles	0.05
PSE0.1		0.1

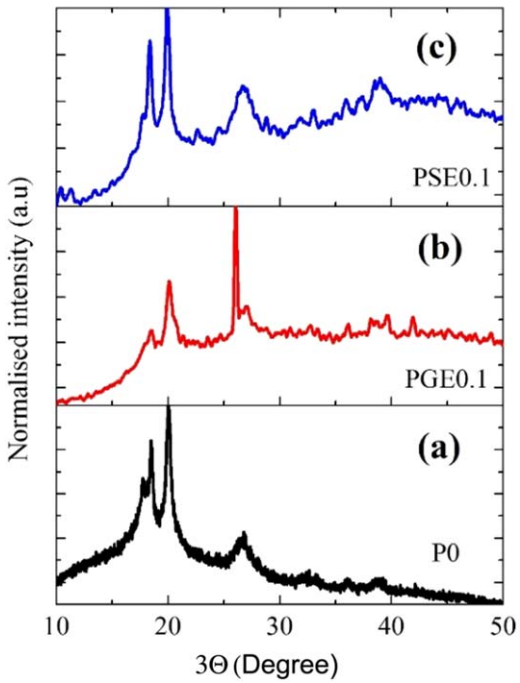

Figure 2. XRD histogram of the samples (a) P0; (b) PGE0.1; and (c) PSE0.1. [Correction made to graphic after initial online publication. 3θ to 2θ]. [Color figure can be viewed in the online issue, which is available at wileyonlinelibrary.com.]

(200) planes]. In Figure 2(b), broadening of the diffraction peaks corresponding to the different phases of PVDF may be described as the decrease in the ordering character of neat PVDF due to the incorporation of the Er^{3+}@GeO_2in PVDF matrix. This may be attributed to the cross-linkage formation within the polymeric material.[1] Similar lowering in crystallinity has also been previously observed for different rare-earth materials loaded PVDF matrix.[1,25] This phenomenon has been reported by the cross-linking between the R^{3+} and the partially

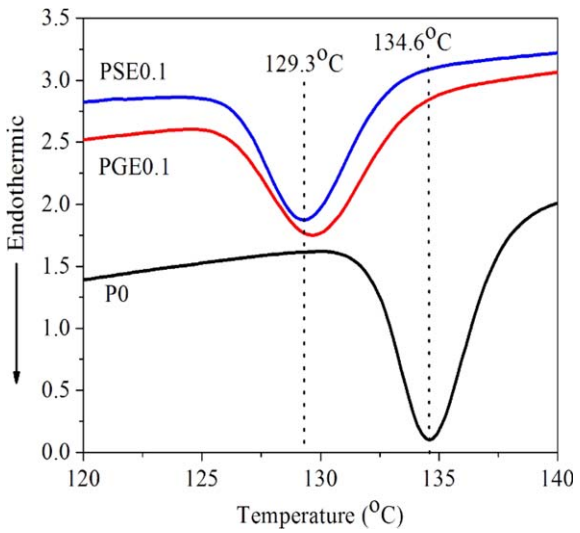

Figure 3. DSC cooling curves of the samples P0, PGE0.1, and PSE0.1. [Color figure can be viewed in the online issue, which is available at wileyonlinelibrary.com.]

negative —CF_2— group of PVDF[1] Figure 2(c) shows the X-ray diffraction pattern of Er^{3+}@SiO_2 loaded PVDF films (PSE0.1). The figure shows an amorphous hump in the lower 2θ region, positioned at 2θ ~ 23° (characteristic hump of SiO_2 nanoparticles)[17] suggesting the successful inclusion of amorphous SiO_2 nanoparticles in PVDF matrix. To have a clear idea about the decrease in the ordering character of the loaded polymer samples DSC measurement of the neat PVDF and the loaded PVDF films are carried out [temperature range: 30–200 °C with a scanning rate 10 °C /min in nitrogen gas atmosphere using DSC-60, Shimadzu (Asia Pacific) Pte. Ltd, Singapore]. The DSC cooling curves for neat as well as PGE0.1 and PSE0.1 are shown in Figure 3. The calculated values of degree of crystallinity for these samples are tabulated in Table II. The results show a clear decrease in the degree of crystallinity for the sample PGE0.1 and PSE0.1 in comparison to the neat PVDF. Our previous study[17] reveals the fact that incorporation of the semiconductor oxide nanoparticles leads to the enhancement of electroactive β phase, which results appearing of peaks at 20.3° and 36.7° corresponding to β phase. But no such prominent peaks corresponding to the β phase of PVDF has been observed in our present observation where rare earth doped semiconductor oxide nanoparticles are being used as filler. The DSC cooling curves also support the phenomenon.[16] This phenomenon may be described by the combined and mutually opposing effects of the positively charged rare earth Er^{3+} ions and the negatively charged semiconductor oxide nanoparticles on the orientation of the polymer chain. Since the positively charged Er^{3+} ion which are being attached to the nanoparticles and the negatively charged nanoparticles tries to orient the polymer chain in opposite directions which retard the all trans or "TTT" confirmation of the PVDF and leads to a mixed α and β phase for the samples. The schematic diagram shown in Figure 4 reveals probable interaction mechanism between the PVDF chains with the added fillers.

Structure and Morphology by TEM and FESEM

Figure 5(a–c) exhibits the FESEM micrographs of the neat PVDF film, PGE 0.1, and PSE 0.1 films, respectively. A uniform and highly compact morphology can be seen from the FESEM image of the neat PVDF (P0). In Figure 5(b), the surface morphology of the Er^{3+}@GeO_2/PVDF nanocomposite film reveals the successful inclusion of cube like GeO_2 NPs in PVDF matrix. A thin layer of PVDF can be seen over the embedded particles. Relatively larger sized GeO_2 particles at the surface of the as synthesized film are found due to the agglomeration of GeO_2 NPs. The successful inclusion and homogeneous dispersion of

Table II. Details of the Degree of Crystallinity of the as Synthesized PVDF Composite Films

Name of the sample	Degree of crystallinity (X_c) = $\frac{\Delta H_c}{\Delta H_{100}\%}$ where $\Delta H_{100}\% = 104.6$ J/g[31]
P0	35%
PGE0.1	34.09%
PSE0.1	22.71%

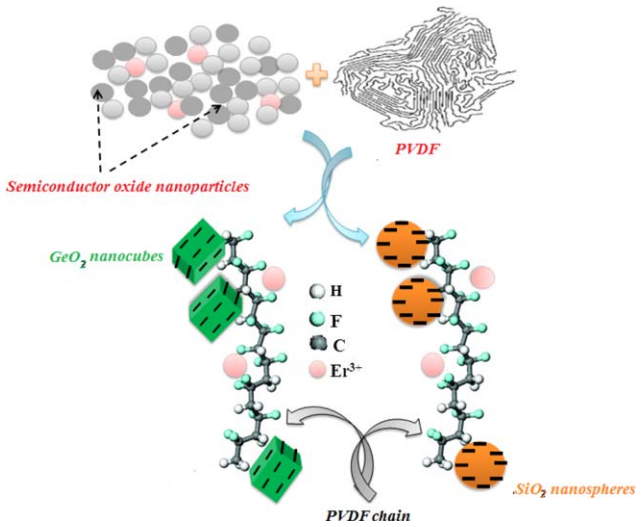

Figure 4. Schematic diagram of the proposed interaction mechanism between the filler and the polymer chain. [Color figure can be viewed in the online issue, which is available at wileyonlinelibrary.com.]

spherical $Er^{3+}@SiO_2$ NPs in PVDF matrix can be observed from Figure 5(c). $Er^{3+}@SiO_2$ NPs were found to be uniformly and discretely distributed all over the polymer matrix without showing any distinct agglomeration.

Figure 6(a,b) reveals the TEM micrographs of the $Er^{3+}@GeO_2$and $Er^{3+}@SiO_2$ NPs infused in PVDF matrix, respectively. The cubic shape of the GeO_2 host particles is clearly seen from Figure 6(a), whereas, the SiO_2 host particles are found to exhibit perfect spherical profile as evident from Figure 6(b). The particle size distribution curves from these TEM micrographs for both the nanoparticles were obtained by using "Image J" software. The diagonal length of a cubic GeO_2 nanoparticle is found to be about 133.5 nm. On the other hand, the average diameter of the SiO_2 host nanoparticles in the PVDF matrix is found to be about 71 nm. The presence of the polymer PVDF as the encapsulating agent is clear from the brighter out-side rings surmounting the darker $Er^{3+}@GeO_2$ and $Er^{3+}@SiO_2$ nanoparticles. However, the presence of Er^{3+} ions is not notable from the TEM micrographs, due to their small quantity in the host matrix and ionic nature.

Energy Dispersive X-ray Spectra Analysis

The results obtained from EDS analyses of the samples PGE0.1 and PSE0.1 are shown in the insets of the Figure 5(b,c), respectively, which validate the successful inclusion of rare earth material erbium in the synthesized composite films. The presence of the GeO_2 and SiO_2 nanoparticles in the composite films can also be seen from Figure 5(b,c). Thus, it can be concluded that, in addition to the polymeric sole component, that is, carbon and fluorine, only erbium and semiconductor oxides (GeO_2 or SiO_2) are present in the samples PGE0.1 and PSE0.1.

Optical Properties

Figure 7(a,b) reveals the UV–Visible absorption spectra of the neat PVDF (P0), $Er^{3+}@GeO_2$/PVDF(PGE), and $Er^{3+}@SiO_2$/PVDF(PSE) nanocomposite films respectively at room temperature in the wavelength region 450–1000 nm. The UV–Vis absorption spectrum for neat PVDF shows almost no absorbance in the higher wavelength region (700–1000 nm).Similar results have also been reported for neat PVDF[32] elsewhere. The UV–Visible absorption spectra for the $Er^{3+}@GeO_2$/PVDF nanocomposite and $Er^{3+}@SiO_2$/PVDF nanocomposites films show four characteristic absorption peaks related to Er^{3+} positioned at 485, 522, 540, and 652 nm. These peaks are attributed to the transitions from the ground state $^4I_{15/2}$ to the various excited state like $^4F_{7/2}$, $^2H_{11/2}$, $^4S_{3/2}$, and $^4F_{9/2}$ofEr^{3+}, respectively.[33] Thus the absorption peaks also confirms the presence of $Er(NO_3)_3$ in the form of Er^{3+} ion in the host matrix.[33] The optical energy band gap (E_g) can be determined on the basis of the frequency dependence of the absorption coefficient a from the UV–VIS spectra by using Davis and Mott formula as follows[34]:

$$a(\nu) = \frac{B(h\nu - E_g)^n}{h\nu} \quad (4)$$

where, B is a constant, h is the Plank's constant (6.625×10^{-34} Js), ν is the photon frequency, and n is an empirical index which is equal $1/2$ for a quantum mechanically allowed indirect band transition.[34] Thus, the above relation becomes

$$E_g = h\nu - \left(\frac{ah\nu}{B}\right)^{\frac{1}{2}} \quad (5)$$

The Tauc plot, that is, the plot of $(ah\nu)^{1/2}$ versus photon energy ($h\nu$) for neat PVDF, PGE, and PSE composite films are shown

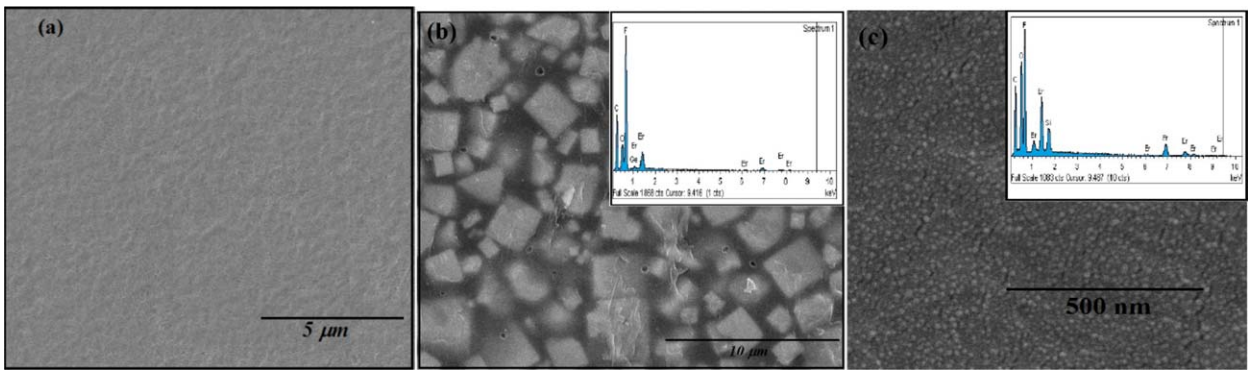

Figure 5. FESEM micrograph of the samples (a) P0; (b) PGE0.1; and (c) PSE0.1. Insets show the EDX spectra of the composite films. [Color figure can be viewed in the online issue, which is available at wileyonlinelibrary.com.]

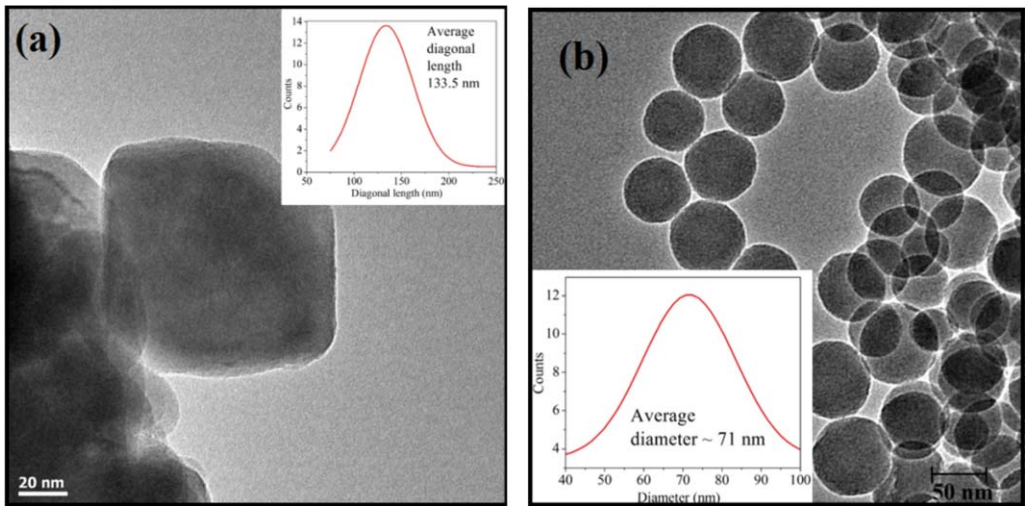

Figure 6. TEM micrograph of the samples (a) PGE0.1; and (b) PSE0.1. Insets show the filler size distribution curve. [Color figure can be viewed in the online issue, which is available at wileyonlinelibrary.com.]

in the Figures 8, 9(a–c), and 10(a–c), respectively. The optical energy gap (E_g) for the allowed indirect transition can be obtained by extrapolating the linear portion of the *a* versus $h\nu$ curves [Figures 8–10(c)] to zero absorption value. The obtained values of E_g for the neat and composite PVDF films are tabulated in Table III. The value of E_g for neat PVDF is about 2 eV, which is in a fair agreement with the E_g value (~2.0 eV) obtained by El-Sayed *et al.* for neat PVDF.[1] The incorporation of erbium doped nanoparticles of 0.02 molar % of Er^{3+} ion consequences significant increase in E_g value; however, no such significant variation is observed for the higher fraction of erbium ions. This behavior may be attributed to the influence of Er^{3+}@GeO_2 and Er^{3+}@SiO_2 on the varying crystallinity of PVDF. The filler added to the polymer matrix can form charge transfer complexes (CTCs) which may provide additional binding energy to the composites resulting in an increase in the E_g value. However, this typical behavior of the E_g value may also be assigned to the change of the induced energy states due to the change in chilation mode up to the filling level 0.02 molar %.[35] Similar result has also been reported by Abdelrazek *et al.* for the LiBr and $MnCl_2$ loaded PVDF films.[36]

Dielectric Studies

Frequency and Temperature Dependence of Dielectric Permittivity. Frequency dependence of dielectric permittivity (ε′) at atmospheric pressure and at temperature 403 K for neat, Er^{3+}@GeO_2 and Er^{3+}@SiO_2 loaded PVDF films are shown in Figure 11(a,b). The temperature variations of dielectric permittivity (ε′) at a frequency 100 Hz for neat and loaded PVDF films are shown in Figure 12(a,b). As seen, the dielectric constant for all of the films including neat PVDF (P0) decreases with the increasing frequency for a fixed temperature value. This phenomenon can be attributed to the decreasing number of aligned dipoles contributing toward polarization[24] with increasing frequency. However, the decrease in dielectric constant with frequency for the loaded PVDF films can also be attributed to the interfacial polarization occurring between the filler and the polymer matrix. At higher frequency the periodic reversal of the applied electric field occurs so fast that there is no excess ion diffusion along the direction of the field present[37] as a result the polarization due to the charge accumulation at the interfaces decreases, leading to the decrease of ε′.

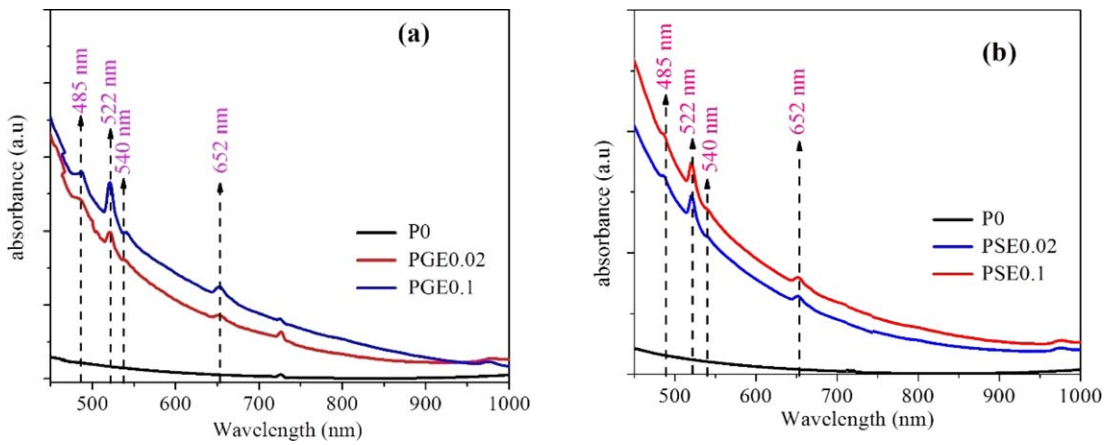

Figure 7. UV–Visible absorption spectra of the samples (a) P0; PGE0.02; PGE0.1 and (b) P0; PSE0.02; PSE0.1. [Color figure can be viewed in the online issue, which is available at wileyonlinelibrary.com.]

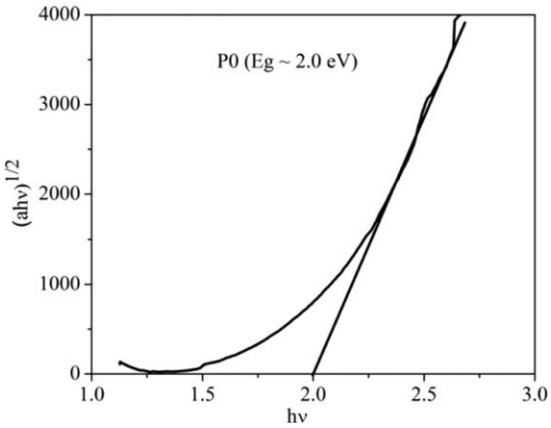

Figure 8. The plot of $(ahv)^{1/2}$ versus photon energy (hv) for neat PVDF (P0).

The dielectric constant for all of the as synthesized PVDF composite films increases significantly with the increasing temperature which is the signature behavior of the strong polar polymer films.[37] The observed significant increase in dielectric permittivity for the filler loaded PVDF films specially at higher temperature and lower frequency is the characteristic phenomenon of Maxwell–Wagner–Sillars (MWS) interfacial polarization which occurs due to the accumulation of electric charges in the discontinuous interfaces between the different phases of the heterogeneous medium having different dielectric permittivity as well as conductivity. When an external electric field is applied on the samples the charges are being accumulated to form space charges which results in a short range dipole–dipole interaction at the filler–polymer interfaces. As a consequence an effective large interfacial polarization occurs resulting in a high dielectric constant at low frequency and high temperature. At higher temperatures, the effect of $Er^{3+}@GeO_2$ loading in PVDF matrix leads to higher value of ε' than that of the $Er^{3+}@SiO_2$ loaded PVDF films and as a result, the maximum value of dielectric constant is obtained for the sample PGE0.1 about approximately 440 at temperature 403 K. Whereas the maximum value of dielectric constant is about approximately 308 found for the sample PSE0.1 films at 403 K. It is worthwhile to mention here that the maximum measured values of dielectric constant for the GeO_2 and SiO_2 loaded PVDF films (15 wt % loading) at the temperature 403 K are approximately 25.25 and approximately 38.34, respectively. Thus it may be inferred that the Er^{3+} shows a predominant effect on the dielectric properties at higher temperature.This typical temperature dependent characteristic of PGE and PSE films may be explained by the combined effect of the loaded fillers' size and the complexes formed. As evident from the TEM micrographs in Figure 6(a,b), polymer shells are formed around the $Er^{3+}@GeO_2$ and $Er^{3+}@SiO_2$ nanoparticles. The formation of the immobilized polymer shells around the nanoparticles restricts the mobility of the PVDF chains at higher temperatures.[24] The larger sized GeO_2 nanoparticles may lead to the formation of larger immobile complexes than that of the smaller sized spherical SiO_2 nanoparticles. As a consequence, at higher temperature a higher value of dielectric constant is obtained for the $Er^{3+}@GeO_2$/PVDF films than that of the $Er^{3+}@SiO_2$/PVDF films.

Dependence of Dielectric Permittivity on Filler Content. Figure 13(a,b) demonstrate the variation of dielectric permittivity (ε') as a function of erbium loading for $Er^{3+}@GeO_2$/PVDF composite films at frequencies 100 Hz, 1 KHz, 10 KHz, and 100 KHz at 300 and 403 K, respectively. Similar variations for the $Er^{3+}@SiO_2$/PVDF composite films are shown in the Figure 14(a,b). It can be seen from the figures that the value of dielectric constant increases with the increasing molar fraction of erbium ion in GeO_2 and SiO_2 nanoparticles which have been loaded in the PVDF matrix. This typical behavior may be attributed to the MWS interfacial polarization as well as increasing crosslinking density of the polymer. The enhancement might be attributed to the presence of the rare-earth material erbium with unique electronic structure which helps in the formation of the immobilized polymer shells around the Er^{3+} ions in the host PVDF matrix.

The erbium ions added to the semiconductor oxide nanoparticles namely GeO_2 and SiO_2 will reside in the nanoparticle matrix. At lower molar fraction of erbium the interfacial polarization occurs predominantly in between the negatively charged surfaces of the semiconductor oxide nanoparticles and polymer matrix contributing toward the enhancement of dielectric constant in comparison to the neat PVDF. In addition to that the formation of complexes by the formation of immobilized polymer shells around the Er^{3+} ion by cross linkage mechanism also contributes toward enhancing the value of dielectric

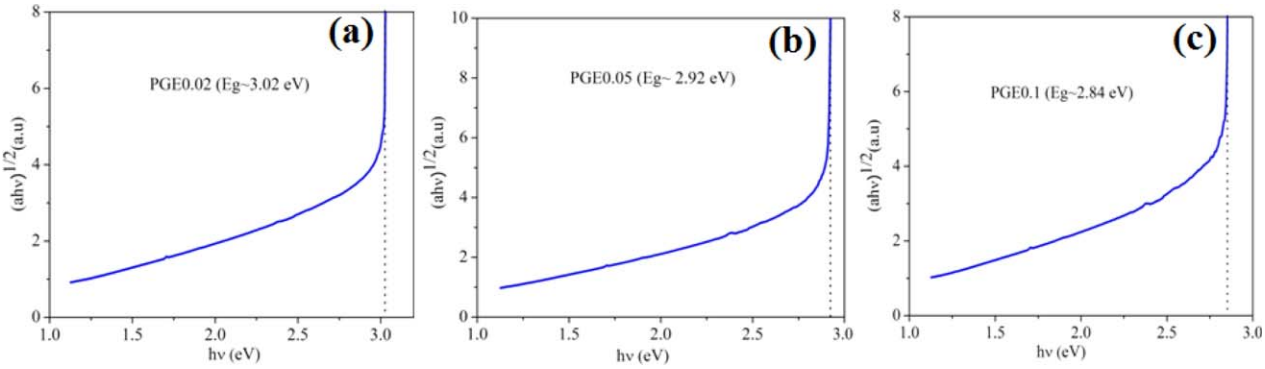

Figure 9. The plot of $(ahv)^{1/2}$ versus photon energy (hv) for the samples (a) PGE0.02; (b) PGE0.05; and (c) PGE0.1. [Color figure can be viewed in the online issue, which is available at wileyonlinelibrary.com.]

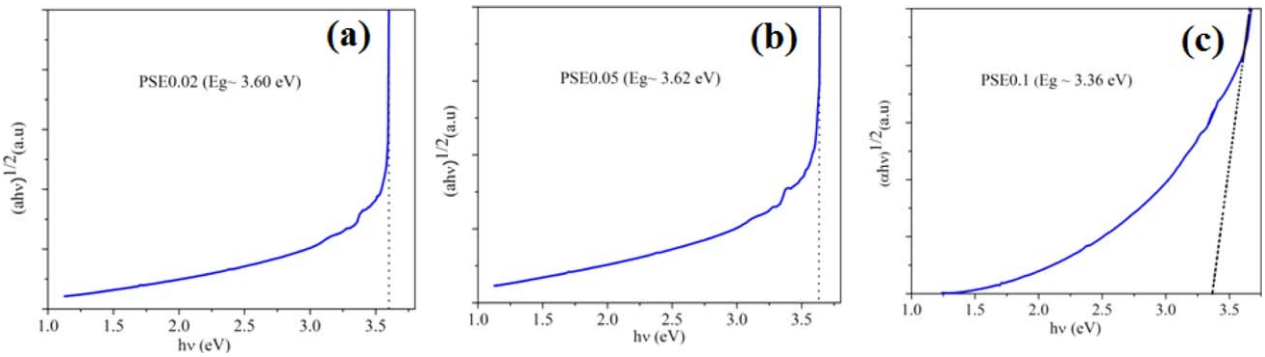

Figure 10. The plot of $(ahv)^{1/2}$ versus photon energy (hv) for the samples (a) PSE0.02; (b) PSE0.05; and (c) PSE0.1. [Color figure can be viewed in the online issue, which is available at wileyonlinelibrary.com.]

Table III. Optical Energy Band Gap (E_g) for the as Synthesized PVDF Composite Films

Name of the sample	Value of the optical energy band gap (E_g) in eV
P0	2.00
PGE0.02	3.02
PGE0.05	2.92
PGE0.1	2.84
PSE0.02	3.60
PSE0.05	3.62
PSE0.1	3.36

permittivity. However, the changes in dielectric constant for Er^{3+}@GeO_2/PVDF films were most prominent for lower erbium content at various frequencies. For higher erbium content, namely 0.02–0.1% the increase in dielectric constant is not so significant. On the other hand, Er^{3+}@SiO_2/PVDF films, also shows an increment in the dielectric constant with the increasing molar fraction of erbium loading at different frequencies. When, the molar concentration of erbium ion increases the number of immobilized polymer shells around the rare-earth ion increases leading to an increasing crosslinking density. At higher molar fraction of erbium, this immobilized polymer shells may be formed around the Er^{3+} ions as well as Er^{3+}@GeO_2 or Er^{3+}@SiO_2nanoparticles.The electronegative fluorine atoms in the polymer chain pull away the electrons from carbon by its –I effect (negative Inductive effect) resulting in electropositive carbon atoms. This polar —CF_2 groups then undergo a columbic interaction with the electropositive Er^{3+} ions, thereby forming polymer shell which encapsulates the Er^{3+} ion.[24] Again, these polymer shells can also be formed around the Er^{3+}@GeO_2 or Er^{3+}@SiO_2 nanoparticles depending upon the localized charge fields of Er^{3+}@GeO_2 and Er^{3+}@SiO_2. Similar contribution of the cross-linking mechanism toward the endorsement of the dielectric constant for the rare-earth loaded PVDF and PVA matrices has also been reported earlier.[38]

For the PGE composites at 300 K, the sample PGE0.1 shows the maximum value of dielectric constant (ε′) which is found to be approximately 19 at 100 Hz. With increasing frequency, a decrease in dielectric constant is observed, and the minimum dielectric constant for the PGE0.1 film is found to be approximately 12.6 at 100 kHz at 300 K. However the maximum value of dielectric permittivity at 300 K has been observed for the

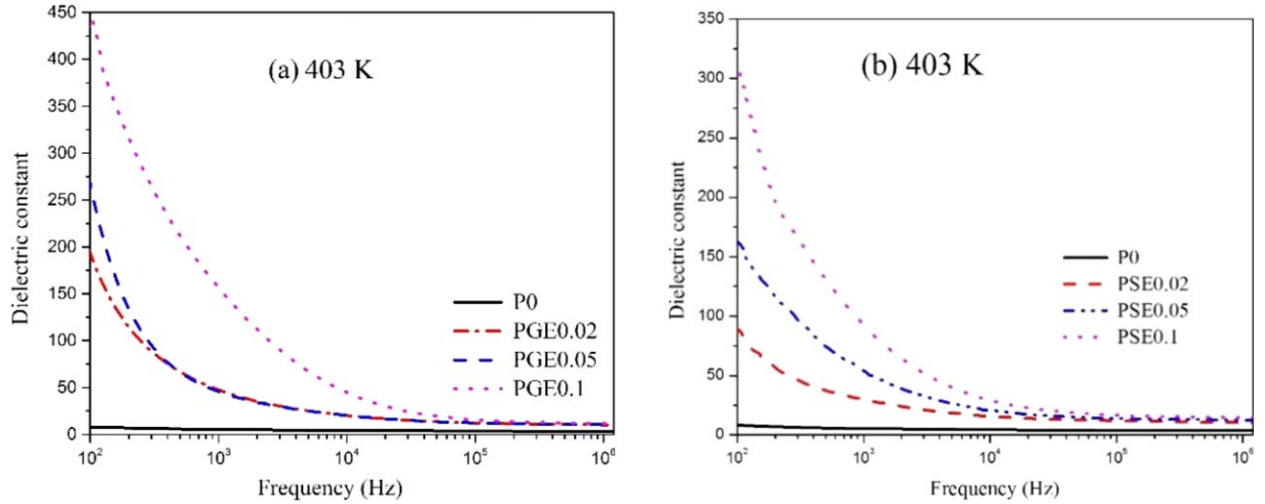

Figure 11. Frequency dependence of dielectric constant at 403 K of the samples (a) P0, PGE0.02, PGE0.05, PGE0.1; and (b) P0, PSE0.02, PSE0.05, PSE0.1. [Color figure can be viewed in the online issue, which is available at wileyonlinelibrary.com.]

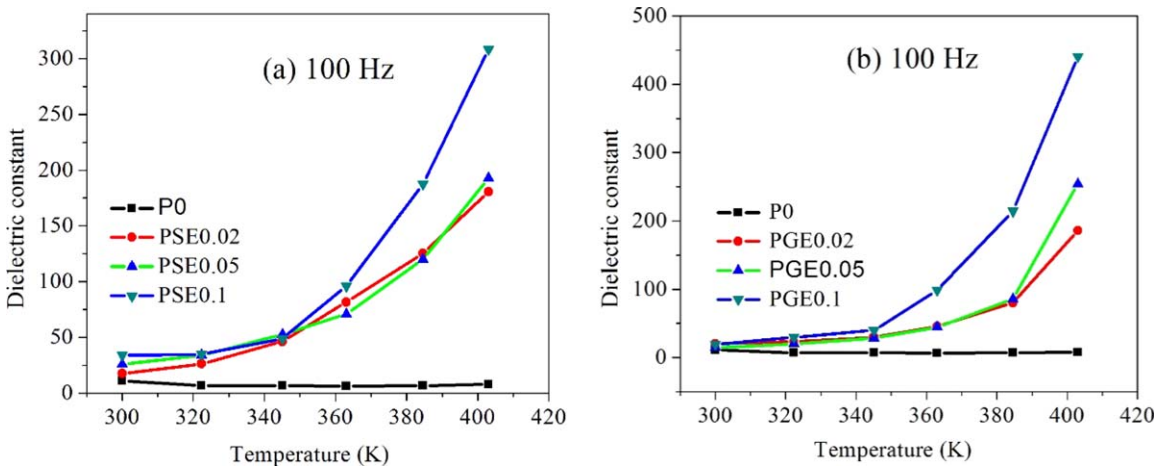

Figure 12. Temperature variation of dielectric constant at 100 Hz of the samples (a) P0, PSE0.02, PSE0.05, PSE0.1 and (b) P0, PGE0.02, PGE0.05, PGE0.1. [Color figure can be viewed in the online issue, which is available at wileyonlinelibrary.com.]

sample PSE0.1 (ε′ at 100 Hz). In this case also, a lowering in dielectric constant value with increasing frequency is evident. Neat PVDF is found to show the lowest dielectric constant values at all frequencies and temperatures. It can also be seen from the Figures 13(a) and 14(a) that the maximum value of the dielectric constant (at 300 K) obtained for the sample PGE0.1 is smaller than that of PSE0.1.This observation can be readily described by the size and the distribution of the loaded particles in the PVDF matrix. The smaller size of the SiO_2 nanoparticles than that of the GeO_2 leads to a more homogeneous and discrete dispersion of Er^{3+}@SiO_2 than the Er^{3+}@GeO_2 in the PVDF matrix as revealed by the Figure 6(c,b). The smaller size of the host oxide semiconductor results in higher charge density. This also leads to a higher surface-to-volume ratio and larger amount of effective interfacial interactions between the added Er^{3+}@SiO_2 fillers and the host PVDF matrix resulting in a higher value of interfacial polarization and crosslinking density.

Frequency Dependence of Tangent Loss (tan δ). Figures 15 and 16(a–c) illustrate the frequency dependence of tangent loss (tan δ) for the samples P0, PGE0.02, PGE0.05, and PGE0.1 respectively at different temperatures. The figures for all the PGE films and neat PVDF reveal that, tan δ decreases with increasing frequency. This typical behavior of tan δ may be attributed to MWS interfacial polarization occurring between the fillers and the PVDF matrix. Due to the low mobility of the charge carriers,[37] they take a relatively longer time to reach the filler–polymer interface and the interfacial polarization also requires long time to take place. As a consequence, the tangent loss possesses higher value at low frequency and decreases with increasing field frequency.[37] The frequency dependence of tangent loss for neat PVDF (Figure 15) shows a relaxation region which may be assigned to the α_c type of relaxation.[38] This α_c relaxation process lies in the 10^1-10^5 Hz frequency domain.[39] This type of relaxation may be assigned to the molecular motions in the PVDF crystalline region. In addition to that, this process is associated with various forms of imperfections in the composite matrix, about chain loops at the lamellar surfaces, chain rotation, and twisting within the interior of the crystal discontinuous defects.[39] This relaxation is being confined in the

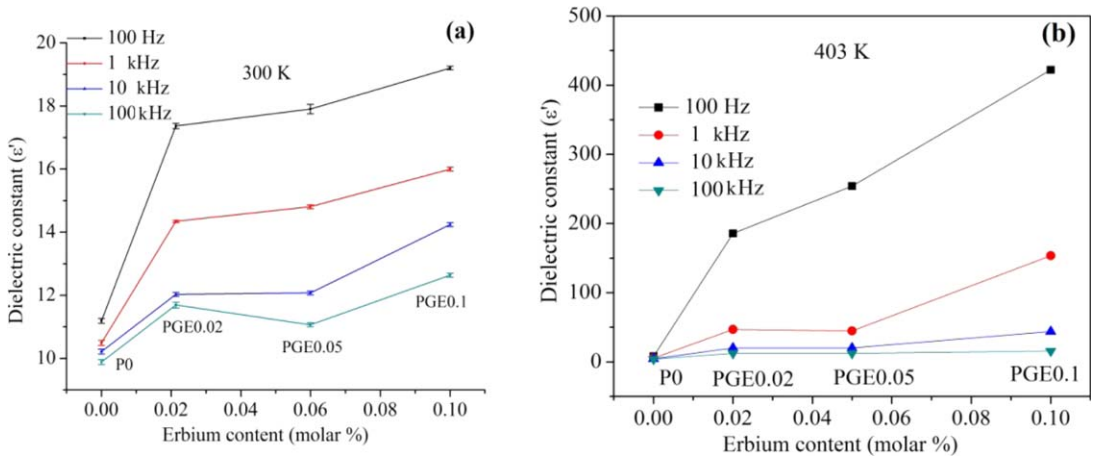

Figure 13. Variation of dielectric constant of the PGE composite films with the loading concentration of Er^{3+} ion considering frequency as parameter at temperature (a) 300 K; (b) 403 K. [Color figure can be viewed in the online issue, which is available at wileyonlinelibrary.com.]

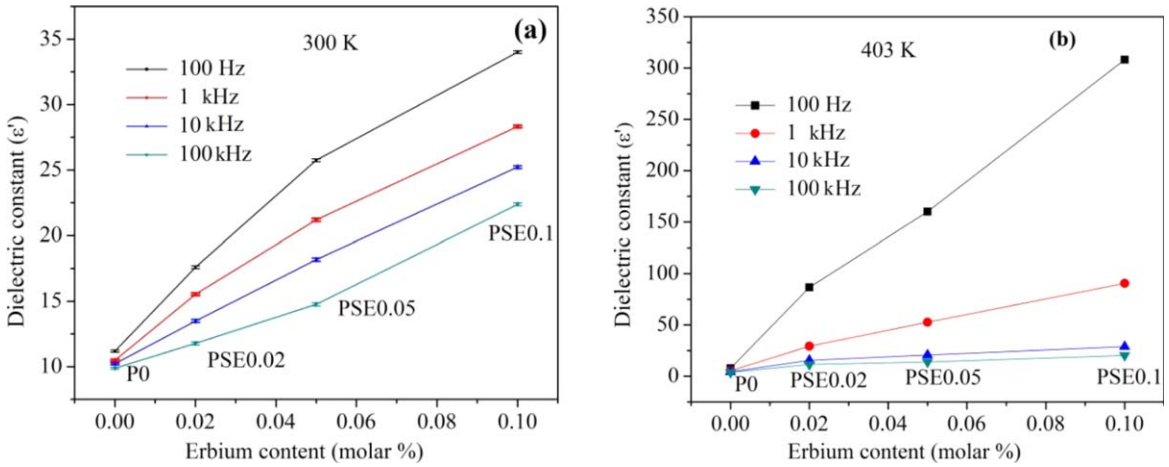

Figure 14. Variation of dielectric constant of the PSE composite films with the loading concentration of Er^{3+} ion considering frequency as parameter at temperature (a) 300 K; (b) 403 K. [Color figure can be viewed in the online issue, which is available at wileyonlinelibrary.com.]

crystalline region of PVDF as a consequence its appearance and growth is a direct result of the development of the crystalline phases. The relaxation peaks, attributed to the α_c relaxation process show increment in magnitude as well as shifting toward higher frequency with the increasing temperature. This is one of the characteristic features of this α_c relaxation process.[26] The frequency dependence of tan δ for the Er^{3+}@GeO_2 loaded PVDF films [Figure 16(a–c)] also reveal the presence of this relaxation process similar to neat PVDF. It can be clearly seen from the Figure 16(a–c) that the α_c relaxation process shows significant peaks for the PGE composites in the frequency range of 10^1-10^5 Hz below the melting temperature (425 K) of the host matrix. However, a closer observation to Figure 16(a–c) reveal the shifting of the peaks related to the α_c relaxation process toward the higher frequency side with the increasing molar fraction of erbium ion in the GeO_2 matrix. This may be attributed to the increasing amount of the immobilized polymer shells around the fillers with the increasing molar fraction of erbium.[24] The frequency variation of the tangent losses for the PSE composite films are shown in the Figure 17(a–c). The figures reveal a similar variation as that of the PGE composite films, that is, the tan δ decreases with the increasing frequency. The humps related to the α_c relaxation process also reveal a shifting toward the high frequency region with the increasing temperature.

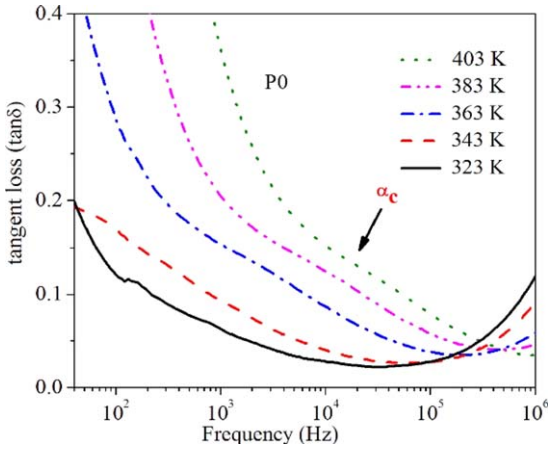

Figure 15. Variation of tangent loss (tan δ) with frequency for the sample P0 at different selected temperatures. [Color figure can be viewed in the online issue, which is available at wileyonlinelibrary.com.]

Frequency and Temperature Dependence of Dielectric Loss (ε″). The temperature and frequency dependence of dielectric loss (ε″) for the samples P0, PGE0.1, and PSE 0.1 are illustrated in a three-dimensional (3D) plot as shown in the Figure 18(a–c). The details variation of dielectric loss for all of the as synthesized PGE and PSE composite films were carried out and since the samples PGE0.1 and PSE0.1 showed significant dielectric behavior, and all other composites showed almost similar variations, results for only the samples PGE0.1 and PSE0.1 have been included in the present manuscript. The frequency dependence of all the samples including neat PVDF showed a step like fall in dielectric loss with the increasing frequency. This 3D plots reveal that the dielectric loss decreases with increasing frequency on the other hand it increases with the increasing temperature. This typical variation of dielectric loss resembles to the power law dissipation of ε′[37] which may be described by the motion of free charge carriers within the composite.[37] The temperature variation of the dielectric loss for all composite films may be attributed to the MWS interfacial polarization which occurs between the loaded fillers and the polymer matrix.

Dependence of Dielectric Loss (ε″) on Filler Content. The variation of dielectric loss (ε″) as a function of erbium molar percentage at different frequencies for the PGE and PSE composite films at two different temperatures namely 300 and 403 K are shown in the Figures 19(a,b) and 20(a,b). The dielectric loss at 300 K for the PGE films [Figure 19(a)] shows a nonlinear behavior with the filler content in the PVDF matrix. It can be seen from the figure that the dielectric loss increases linearly up to 0.02 molar percentage of erbium. Beyond 0.02 molar %, the dielectric loss is found to decrease. This decrease in the

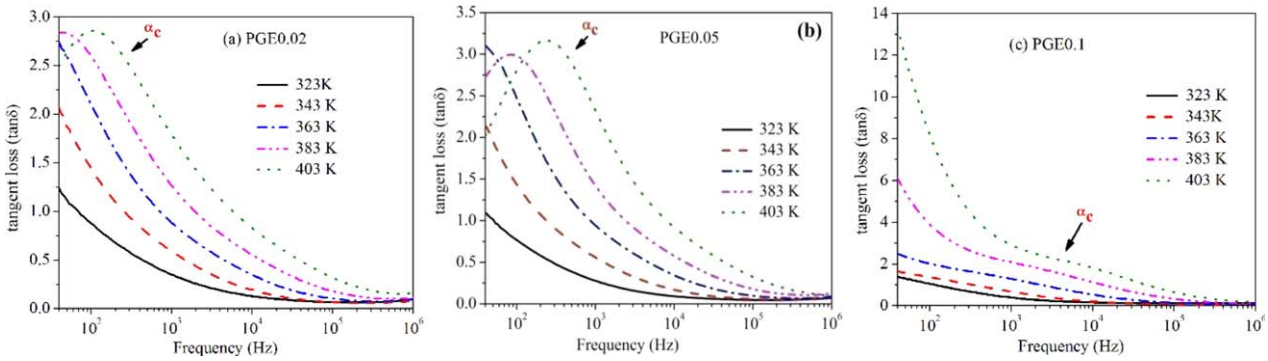

Figure 16. Variation of tangent loss (tan δ) with frequency at different selected temperatures for the samples (a) PGE0.02; (b) PGE0.05; and (c) PGE0.1. [Color figure can be viewed in the online issue, which is available at wileyonlinelibrary.com.]

dielectric loss may be assigned to the phase inversion occurring in the polymer matrix due to the addition of fillers as well as lowering of the leak current at this molar fraction.[16] However, the loss again increases for the higher molar fraction which might be due to the increase in the leak current with the addition of excess erbium ions. Similar type of variation for tangent loss was also reported by Thakur *et al.*[16] The maximum value of dielectric loss (∼7.47) at 300 K is obtained for the sample PGE0.1 at the frequency 100 Hz for the PGE composite films. The content dependence of dielectric loss at higher temperature (403 K) for the PGE composites films is shown in the Figure 19(b), which reveals almost linear increment of dielectric loss with increasing molar concentration of erbium ions in the GeO_2 matrix with a maximum value approximately 2450 at 100 Hz. In Figure 20(a,b), the content variation of the PSE composite films at the temperatures 300 and 403 K shows almost linear increase of the dielectric loss with increasing erbium molar fraction. The maximum values of dielectric loss at the both temperatures are obtained for the samples PSE0.1, which are about 9.0 and 1400, respectively.

Electric Modulus

The polarization which is responsible for the high value of the dielectric constant at lower frequency and high temperature is the interfacial polarization. Though this polarization is almost always occurs in polymeric composites but it is hidden by the electrical conductivity. To overcome this difficulty to observe the presence of interfacial polarization, the electric modulus formalism can be used to analyze the electrical conductivity in such polymeric composites. In addition to that, this modulus formalism can also suppress the signal intensity related with the electrode polarization, emphasizing small features at high frequency. Due to these advantages, this procedure can be used to determine different charge carrier parameters like conductivity relaxation time.[24] The complex electric modulus (M^*) is defined as the inverse of the complex dielectric permittivity (ε^*) and can be expressed in terms of the dielectric constant (ε') and dielectric loss (ε'') as follows:[24]

$$M^* = \frac{1}{\varepsilon^*} = \frac{\varepsilon'}{\varepsilon'^2 + \varepsilon''^2} + i\frac{\varepsilon''}{\varepsilon'^2 + \varepsilon''^2} \quad (6)$$

$$M^* = M' + iM'' \quad (7)$$

where, M' and M'' are the real and imaginary part of the complex electric modulus, M^*.

Frequency Variation of Real Part of Electric Modulus (M′). Figure 21(a,b) represent the variation of M' as a function of frequency at different fixed temperatures for samples PGE0.02 and PGE0.1, respectively. The same variation for the PSE films is illustrated in Figure 22(a,b). It can be seen from the figures that for all of the loaded PVDF films, M' increases with the increasing frequency with a typical "S" shaped pattern which is typical for such polymeric materials like PVDF.[24] However, the enhancement in the value of M' can be attributed to

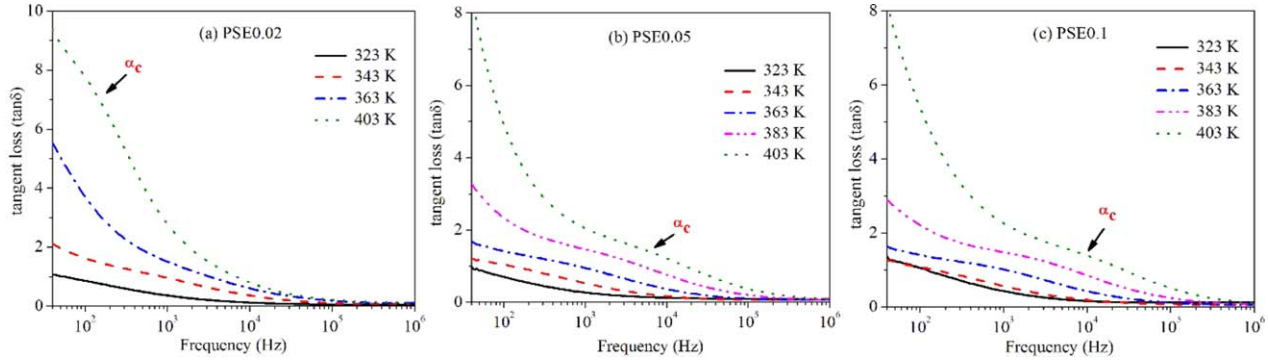

Figure 17. Variation of tangent loss (tan δ) with frequency at different selected temperatures of the samples (a) PSE0.02; (b) PSE0.05; and (c) PSE0.1. [Color figure can be viewed in the online issue, which is available at wileyonlinelibrary.com.]

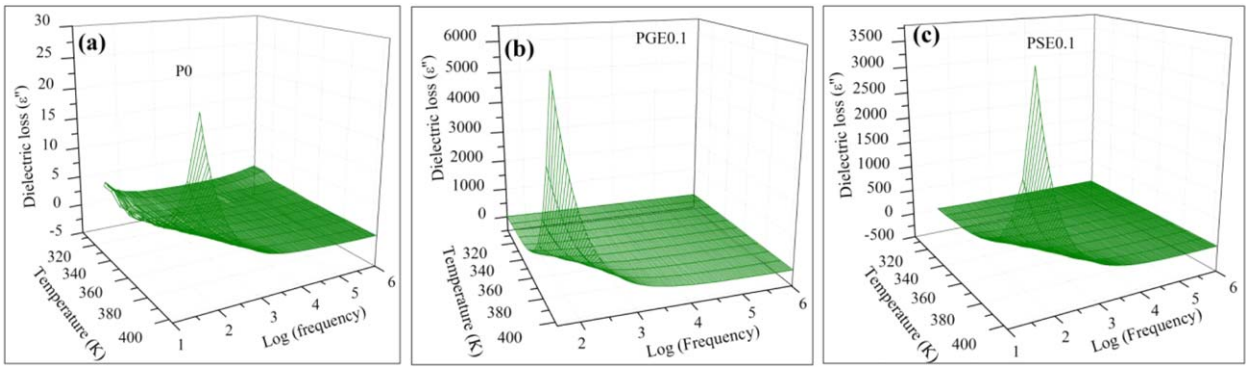

Figure 18. Variation of the dielectric loss (ε″) with frequency and temperature (3D plot) for the sample (a) P0; (b) PGE0.1; and (c) PSE0.1. [Color figure can be viewed in the online issue, which is available at wileyonlinelibrary.com.]

the interfacial polarization effect occurring at the interfaces in the composite films.[24] In addition to that the cross-linking formations in the polymer matrix due to the presence of the rare-earth ions is also responsible for such increment in M' value.It can also be seen from the variations that M' possess near zero values at low frequency and high temperature. This indicates the partial removal of the electrode polarization in the given operating condition region.[24] Thus the results infer that the electrode polarization plays an important role at high temperature and low frequency.

Frequency Dependence of the Imaginary Part of Electric Modulus (M″). The variation of M'' as a function of frequency for the neat PVDF, PVDF films loaded with Er^{3+}@GeO_2 and Er^{3+}@SiO_2 NPs at different selected temperature is displayed in Figures 23–25(a,b), respectively. The variation of M'' for the sample P0 reveals that it undergoes different relaxation processes in the experimental frequency domain. The relaxation process occurring in the lower frequency region may be attributed to the interfacial polarization according to Rekik *et al.*[39] Since PVDF is a semicrystalline polymer so the polarization is occurring between the crystalline and amorphous phase of the polymer.[39] This process is attributed to the micro-Brownian motion in the amorphous region of the main polymer chain. This variation also reveals an enhancement of the contribution of dc conductivity. The second relaxation peak at higher frequency region is attributed to the α_c relaxation process correlated to the molecular motions in the crystalline region of main PVDF polymer chain. The details about the origin of this α_c relaxation process have been discussed in the previous sections. Though the frequency dependence of M'' for neat PVDF displays the presence of two different relaxation processes but the variation for the loaded PVDF films [Figures 24(a,b) and 25(a,b)] show significant enhancement only for those peaks related to the α_c relaxation process. As mentioned before, the signature behavior of this α_c relaxation process (occurring below the melting temperature of the host matrix) is the shifting of the correlated peaks to the higher frequency region with increasing temperature. Similar nature of peak shifting has also been observed for the filler loaded PVDF films. The low frequency region of this M'' peaks signifies the range in which ions can successfully hop to the neighboring sites, while the high frequency side illustrates the range in which the ions are spatially confined to their potential wells and can move only within the well.[1] As a consequence, the frequency regions where the peaks occur indicate the transition from long range mobility to short range mobility

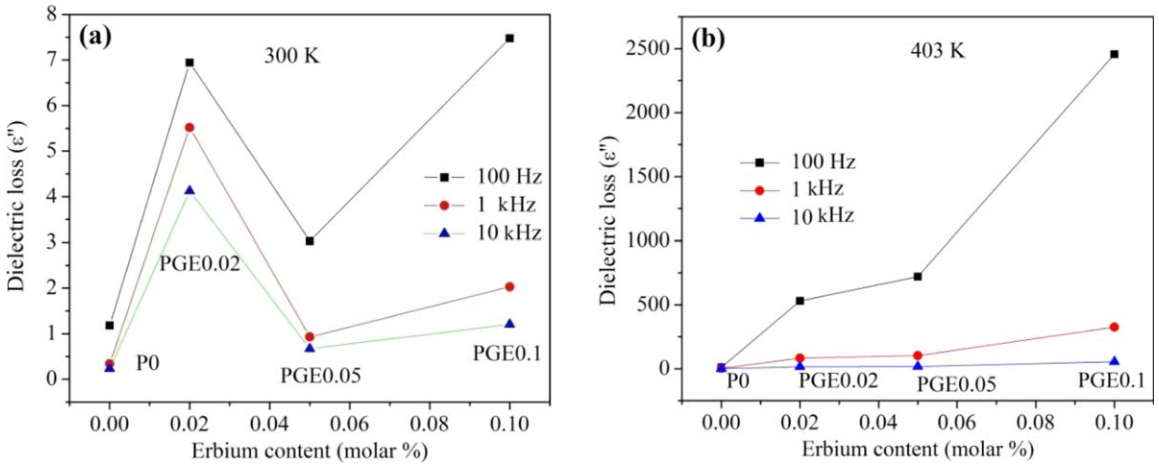

Figure 19. Variation of dielectric loss of the PGE composite films with the loading concentration of Er^{3+} ion at different frequencies for the temperatures (a) 300 K; (b) 403 K. [Color figure can be viewed in the online issue, which is available at wileyonlinelibrary.com.]

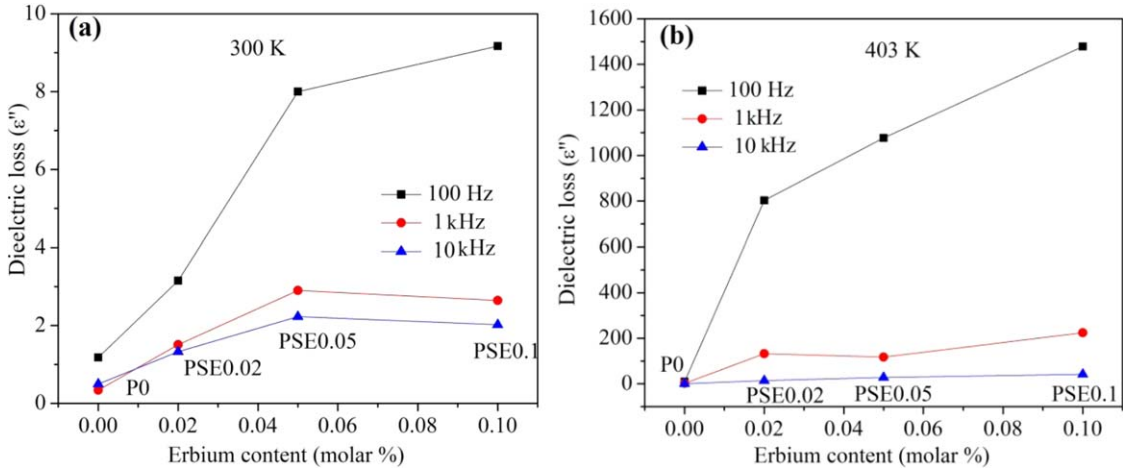

Figure 20. Variation of dielectric loss of the PSE composite films with the loading concentration of Er^{3+} ion at different frequencies for the temperatures (a) 300 K; (b) 403 K. [Color figure can be viewed in the online issue, which is available at wileyonlinelibrary.com.]

with increasing frequency. Again, the bell shape of these peaks is also typical for such ionic materials.[1] This bell shape of M'' may also infer that the conduction mechanism in this case is the temperature dependent hopping process.[1] The frequency dependence of M'' for the loaded PVDF films [Figures 24(a,b) and 25(a,b)] also reveal the lowering of full width at half maximum (FWHM) of this bell shaped relaxation peaks with the increasing temperature, which is attributed to the deviations in the high frequency side of the peak. This electric field relaxation due to the motions of charge carriers is generally well described by the empirical Kohlrausch–Williams–Watts (KWW) function.[1]

$$\varnothing(t) = \exp\left[-\left(\frac{t}{\tau}\right)^{\beta}\right] \tag{8}$$

where, τ and β $\left(=\frac{1.14}{w}\right.$ where, w is the peak value at FWHM[40]$\left.\right)$ are the conductivity relaxation time and the Kohlrauch exponent, respectively. The Debye-type relaxation occurs when the value of β becomes equal to unity. Smaller the value of β, the larger the deviation of the relaxation from the Debye-type relaxation ($\beta = 1$) process.

The conductivity relaxation time τ is defined by the relation $2\pi f_m \tau = 1$. Where, f_m is the frequency at which the maximum M'' occurs. Normally τ exhibit Arrhenius behavior and defined as[24]:

$$\tau = \tau_0 \exp\frac{E_a}{KT} \tag{9}$$

where, E_a is the activation energy of the relaxation process, τ_0 is the relaxation time at infinite temperature, K is the Boltzmann constant, and T is the absolute temperature. Figure 26(a,b) depicts the plot of ln(τ) versus $1000/T$ for pure PVDF films and for the Er^{3+}@GeO_2, Er^{3+}@SiO_2 loaded PVDF films with different molar concentrations of Er^{3+}. The E_a values are calculated from the Figure 26(a,b) and tabulated in the Table IV. It is worthwhile to mention here that the value obtained for the activation energy E_a for neat PVDF (P0) is in fair agreement with the values reported earlier.[24] However, the calculated values of the activation energy also infer that the conduction mechanism is ionic in nature.[24] It can also be seen from Table IV that the value of the activation energy (E_a) decreases with the increasing molar fraction of Er^{3+} ion in the semiconductor oxide matrix. Similar variation of activation energy has been obtained by Sayed *et al.* for

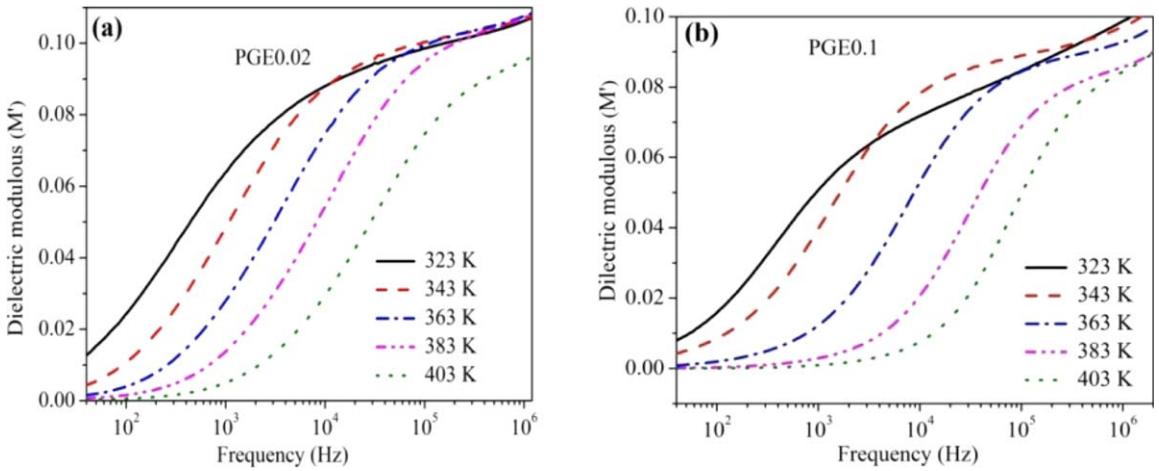

Figure 21. Variation of M' with frequency of the samples (a) PGE0.02; and (b) PGE0.1. [Color figure can be viewed in the online issue, which is available at wileyonlinelibrary.com.]

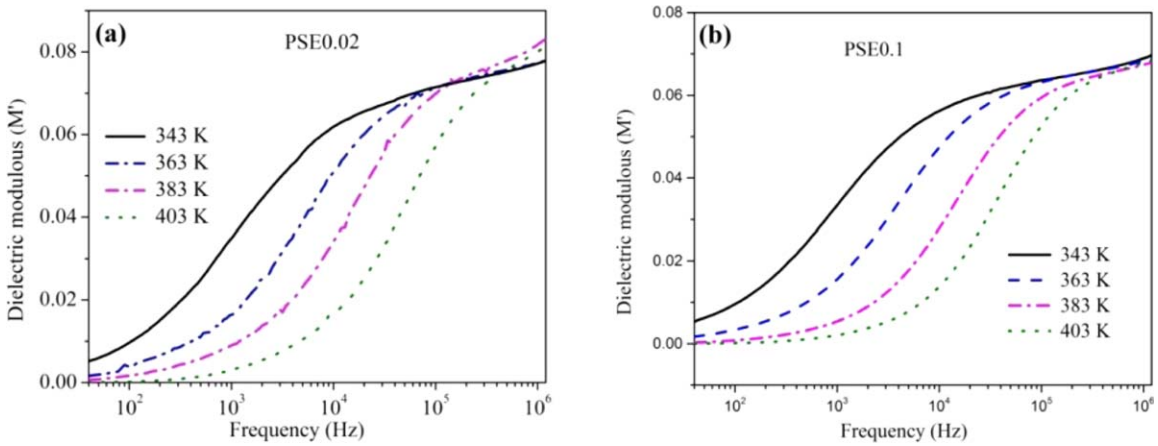

Figure 22. Variation of M' with frequency of the samples (a) PSE0.02; and (b) PSE0.1. [Color figure can be viewed in the online issue, which is available at wileyonlinelibrary.com.]

$GdCl_3$ loaded PVDF films.[1] This decrease in the activation energy with the increasing molar fraction of erbium infers that the addition of the erbium ions through semiconductor oxide matrix plays role in favor of the conduction mechanism. The decrease in the activation energy also indicates that the loading of the filler leads to the decrement in the potential barrier height related to the conduction mechanism.

Temperature Dependence of M″. Figure 27(a,b) reveal the temperature dependence of M'' at 100 Hz Er^{3+}@GeO_2 and Er^{3+}@SiO_2 loaded PVDF films respectively. Figure 27(a) displays the presence of a well-defined peak around 343 K for the PGE composite films. A similar peak positioned around 344 K can also be seen for the PSE composite films [Figure 27(b)]. As mentioned in the earlier section, the peak occurring at a temperature below the melting temperature of the host matrix can be ascribed by the α_c relaxation process in the composite.[39] Thus the temperature dependence of this imaginary part (M'') of the complex dielectric modulus (M^*) is also consistent with the behavior of M' (f) for both type filler loaded PVDF matrix, which also supports the presence of the α_c relaxation process in the as synthesized neat and composite films. The figures also illustrate [Figure 27(a,b)] that the magnitude of the α_c relaxation slightly decreases with the increasing molar percentage of Er^{3+} in $GeO_2$and SiO_2 matrices. This small decrease in the magnitude of the α_c relaxation may be explained by the decrease in the ordering pattern of the crystalline phase of PVDF due to the filler loading as reported by Rekik *et al.*[39] This lowering in the degree of order of crystallinity of PVDF may be assigned to the formation of complexes between the filler and PVDF matrix by multiple cross-linking mechanism.[1] In this context, it is worthy to mention that the lowering in crystallinity is also supported by XRD patterns and DSC results obtained for the samples P0, PGE0.1, and PSE0.1.

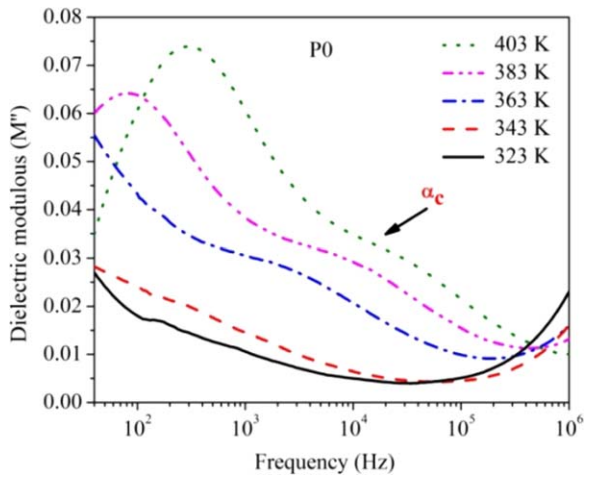

Figure 23. Variation of M'' with frequency of the sample P0. [Color figure can be viewed in the online issue, which is available at wileyonlinelibrary.com.]

ac Conductivity

Frequency Dependence of ac Conductivity. The energy dissipation in a dielectric medium when subjected to an external alternating electric field is related to the electrical conductivity of the medium. The frequency dependent ac conductivity σ* can be calculated from the dielectric permittivity and dielectric loss according to the following standard relations[40]

$$\sigma^* = i\varepsilon_0\ \omega\varepsilon^*(\omega) = i\varepsilon_0\omega(\varepsilon'(\omega) - i\varepsilon''(\omega)) = \varepsilon_0\omega\varepsilon''(\omega) + i\varepsilon_0\omega\varepsilon'(\omega) = \sigma'(\omega) + i\sigma''(\omega) \quad (10)$$

where, $\omega(=2\pi f)$ is the angular frequency.

The above equations show that the real part of the ac conductivity is proportional to the dielectric loss which results due to the flow of charges through the dielectric material known as the dc conduction. However, the imaginary part of the ac conductivity is related to the dielectric permittivity, which does not include the charges that pass through the dielectric material; rather it is generated to compensate the charges which are polarized within the dielectric material. This phenomenon is known as the dielectric dispersion.[41] However, the ac conductivity of the as synthesized samples can be expressed using the standard equation as:

$$\sigma_{ac}\ (f) = \sigma_t - \sigma_{dc} = 2\pi C f^s \quad (11)$$

where, σ_{dc} is the low-frequency conductivity or dc conductivity, σ_t and σ_{ac} are the total conductivity and the ac part

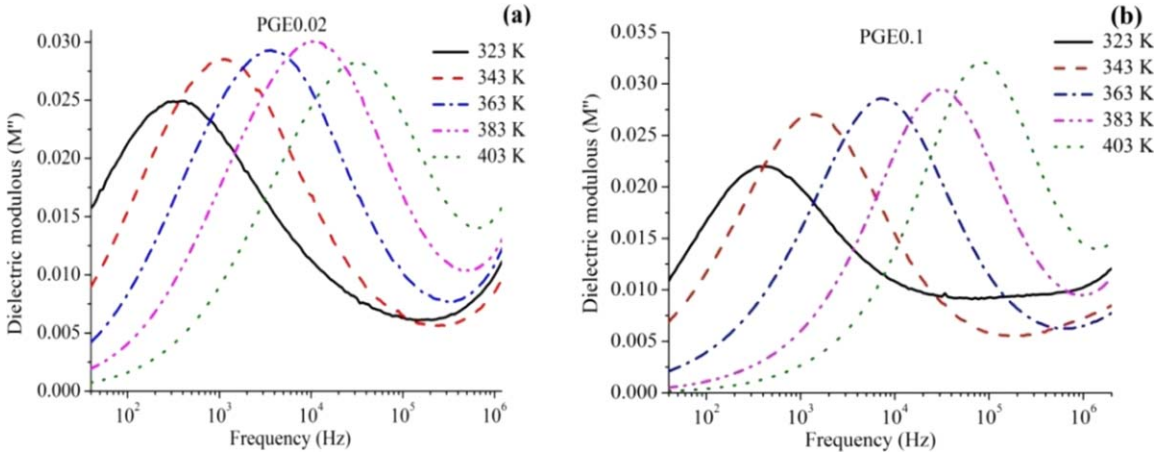

Figure 24. Variation of M'' with frequency of the samples (a) PGE0.02; and (c) PGE0.1. [Color figure can be viewed in the online issue, which is available at wileyonlinelibrary.com.]

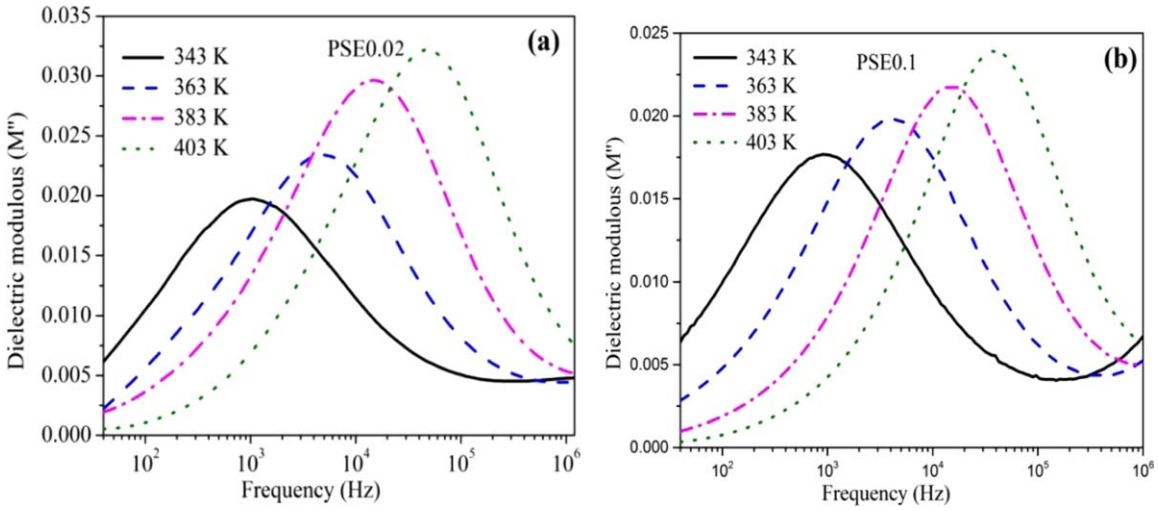

Figure 25. Variation of M'' with frequency of the samples (a) PSE0.02; and (b) PSE0.1. [Color figure can be viewed in the online issue, which is available at wileyonlinelibrary.com.]

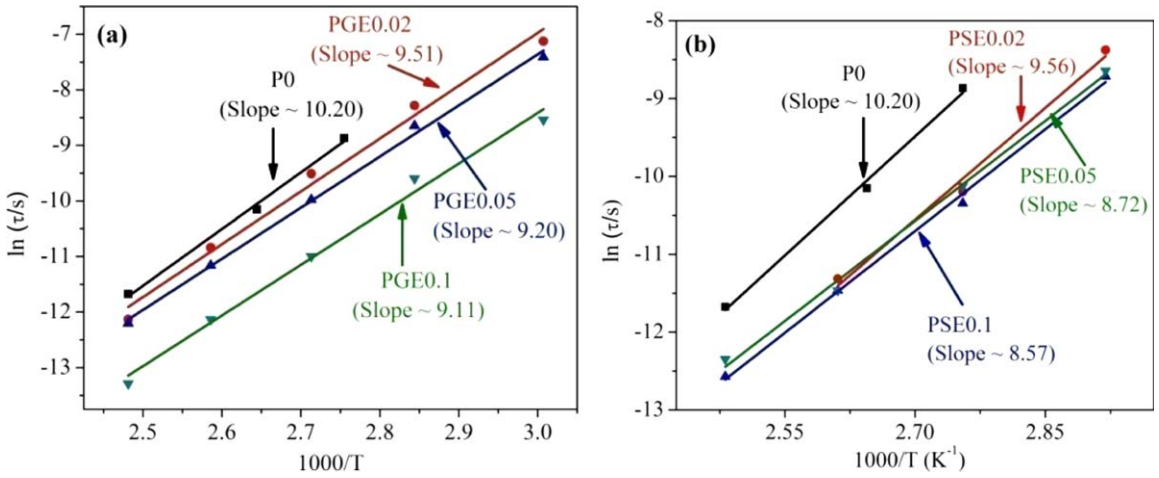

Figure 26. Plot of ln(τ) versus 1000/T for the samples (a) P0, PGE0.02, PGE0.05, and PGE0.1; and (b) P0, PSE0.02, PSE0.05, and PSE0.1. [Color figure can be viewed in the online issue, which is available at wileyonlinelibrary.com.]

Table IV. Activation Energy (E_a) for the α_c Relaxation Process of the as Synthesized Samples

Name of the sample	Activation energy for relaxation (E_a) (eV)	Regression factor (R^2)
P0	0.878	0.9991
PGE0.02	0.819	0.9997
PGE0.05	0.792	0.9996
PGE0.1	0.784	0.9998
PSE0.02	0.823	0.9994
PSE0.05	0.751	0.9993
PSE0.1	0.738	0.9997

of the total conductivity, respectively. C is the pre-exponential factor and s is the exponent factor. The above equation also reveals that the total conductivity is the sum of the dissipative factors, one is the ohomic conduction (σ_{dc}) created by free charges and the second is the frequency dependent dielectric dispersion ($2\pi Cf^s$).[40] The total conductivity of the as synthesized films can be divided into two different regions. The first part is for low frequency which is mainly dominated by the dc conductivity and the second regime is for higher frequencies, characterized by the frequency dependent conductivity or ac conductivity. The dc conductivity can be obtained by extrapolating $\sigma_t(f)$ to $f \rightarrow 0$ and it can be subtracted from the total conductivity to obtain the ac conductivity.

The study of the temperature dependent frequency variation of the conductivity is useful to elucidate the microscopic dielectric relaxation mechanism occurring in the as synthesized samples. Though in the present experimental study the bell-shaped variation of M'' [Figures 24(a,b) and 25(a,b)] with frequency infers the conduction mechanism is ionic in nature, however, there are different models which have been proposed to evaluate the mechanism behind dielectric relaxation. One of them is the quantum mechanical tunneling (QMT) which is related to the tunneling of the electrons or polarons through the barriers separating the localized states. For covalent solids like PVDF, the small polaron tunneling (SPT) model may be applied only

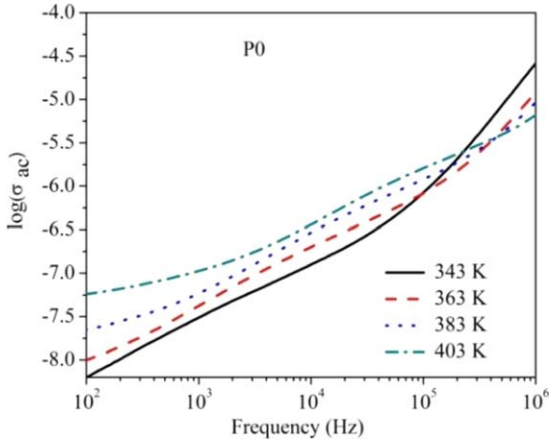

Figure 28. Frequency dependence of ac conductivity (σ_{ac}) of neat PVDF. [Color figure can be viewed in the online issue, which is available at wileyonlinelibrary.com.]

when the addition of a charge carrier to a site causes a large degree of local lattice distribution. Another model, correlated barrier hopping model (CBH) was proposed by Pike[42] for ionic polymers and related to the classical hopping over the barriers.[24]

The frequency dependence of the ac conductivity at different selected temperatures for the samples P0, PGE and PSE composite films are shown in the Figures 28–30(a,b), respectively. The variations indicate that for all of the as synthesized films including the neat PVDF, the ac conductivity increases prominently with the increasing frequency as well as temperature. This increment of σ_{ac} with the frequency may be explained by using the eq. (11) as shown above. With increasing frequency, the mean displacement of the charge carriers is reduced and as a consequence, the ac conductivity of the loaded PVDF films follow the power law of f^s and increases significantly with increasing frequency. Again, this enhancement of the ac conductivity with frequency as well as temperature also is in agreement with the MWS interfacial polarization and also with the dielectric relaxation processes occurring in the composite films. The variations of the ac conductivity for both types of composites

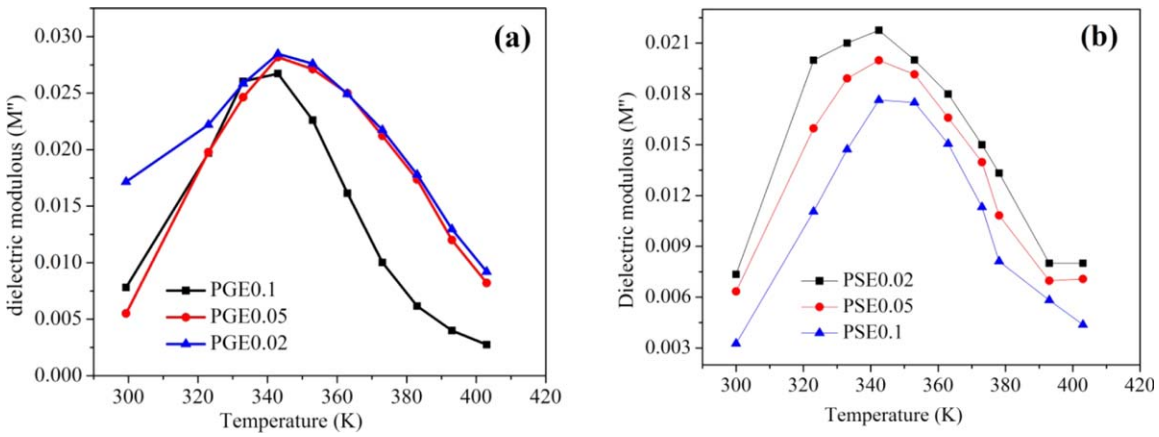

Figure 27. Variation of M'' with temperature for the samples (a) PGE0.02, PGE0.05, and PGE0.1; (b) PSE0.02, PSE0.05, and PSE0.1. [Color figure can be viewed in the online issue, which is available at wileyonlinelibrary.com.]

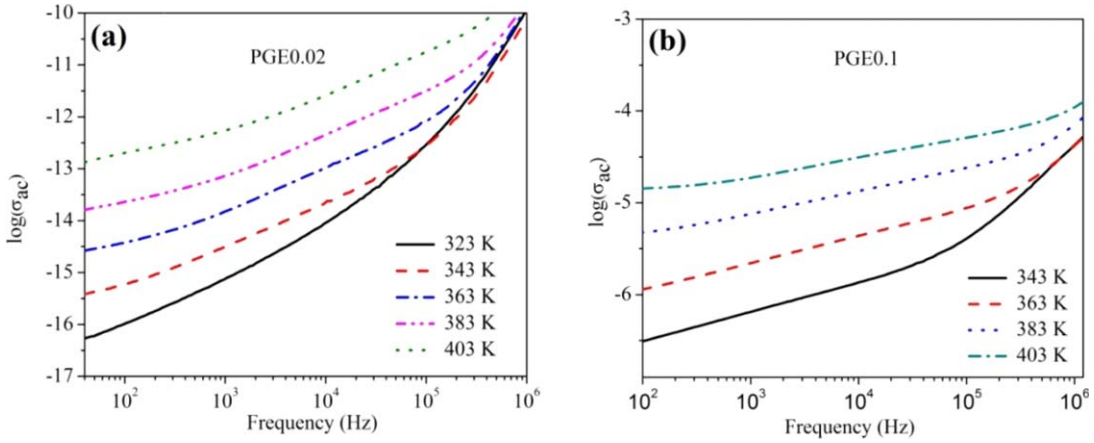

Figure 29. Frequency dependence of the ac conductivity (σ_{ac}) of the samples (a) PGE0.02; and (b) PGE0.1. [Color figure can be viewed in the online issue, which is available at wileyonlinelibrary.com.]

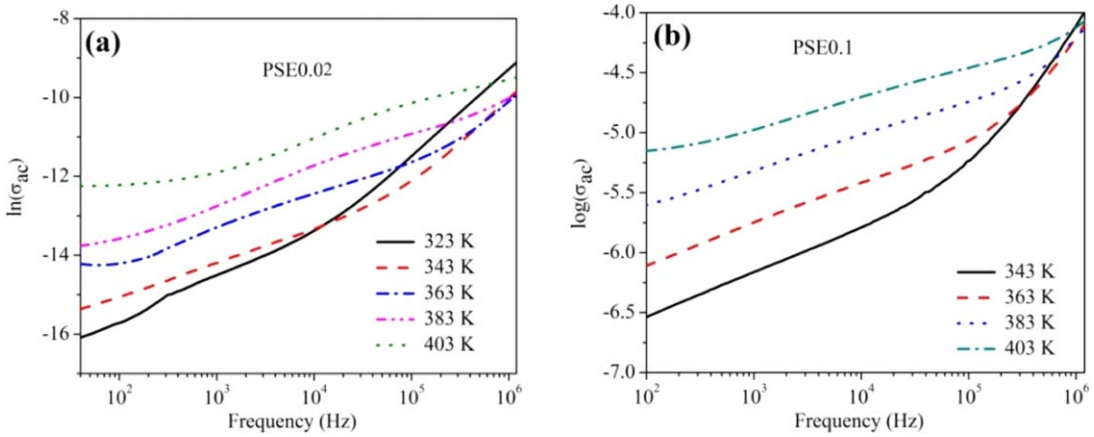

Figure 30. Frequency dependence of ac conductivity (σ_{ac}) of the samples (a) PSE0.02; and (b) PSE0.1. [Color figure can be viewed in the online issue, which is available at wileyonlinelibrary.com.]

show that the conductivity readily increases with the increasing molar fraction of erbium ions for both the composite films at low frequency. A linear behavior with the logarithmic frequency was also observed. These observations suggest significant contribution of fillers on the ac conductivity[40] of the composite films.

To have an idea about the conduction mechanisms occurring in the as synthesized neat and composite PVDF films, the frequency dependence of ac conductivity within the frequency range of the α_c relaxation for the samples P0, PGE0.1, and PSE0.1 are shown in the Figure 31(a–c). The figures yield straight lines with different slope "*s*." The values of "*s*" obtained for the neat PVDF films are consistent with the values earlier reported by Hassen *et al.*[25] The values of "$1 - s$" for the sample P0, PGE0.1, and PSE0.1 at different temperatures are shown in the Figure 32, which shows a decrease in the slope (*s*) value with the increasing temperature for all the samples. Similar

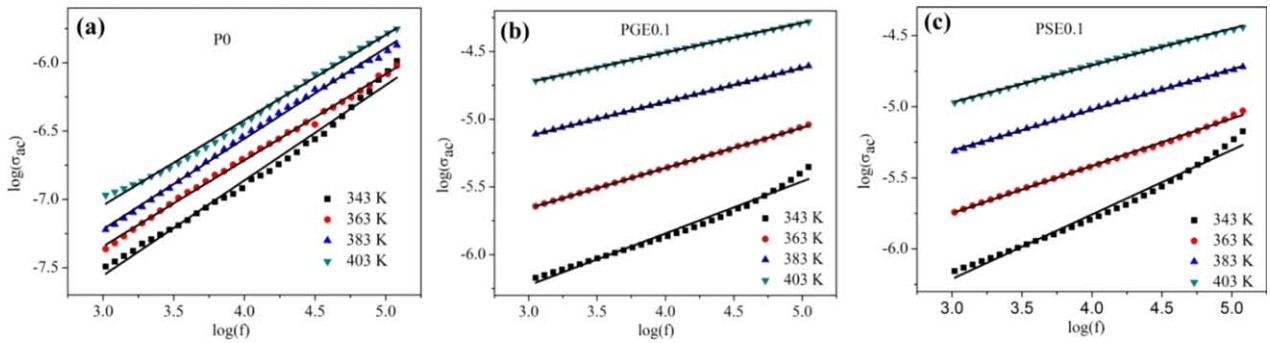

Figure 31. Frequency dependence of ac conductivity (σ_{ac}) in the α_c relaxation region of the samples (a) P0; (b) PGE0.1; and (c) PSE0.1. [Color figure can be viewed in the online issue, which is available at wileyonlinelibrary.com.]

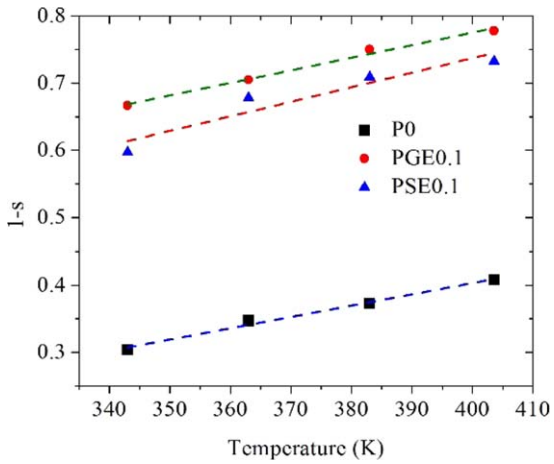

Figure 32. Variation of $(1-s)$ with temperature of the samples P0, PGE0.1, and PSE0.1. [Color figure can be viewed in the online issue, which is available at wileyonlinelibrary.com.]

Table V. Hopping Distance (R) and Binding Energy (W_m) of the as Synthesized Samples

Name of the sample	Hopping distance (R) 300 K (eV)	Hopping distance (R) 403 K (eV)	Binding energy (W_m) (eV)
P0	0.584	0.553	0.44
PGE0.1	0.287	0.266	0.305
PSE0.1	0.324	0.281	0.267

variation of s for the rare-earth material loaded PVDF films has been reported earlier by Kumar *et al.*[26] This typical phenomenon strongly suggests that the conduction mechanism is correlated with barrier hopping,[1] that is, conduction mechanism can be described by the CBH model for our case. Using this CBH model, hopping distance (R) for the conduction of the carriers can be calculated using the universal exponent "s", as[1]:

$$R = \frac{6kT}{1-s} \tag{12}$$

where, k and T are the Boltzmann constant and absolute temperature, respectively. The calculated values of the hopping distance for the neat PVDF, PGE0.1, and PSE0.1 at temperature 300 and 403 K are tabulated in Table V, which shows the hopping distance is shorter for the nanocomposites samples with respect to the neat PVDF. The table also shows that the hopping distance decreases with the increasing temperature. Similar decrease in the hopping distance has already been reported earlier for the $GdCl_3$ loaded PVDF films.[1] Again "s" can also be written in the following form considering the CBH model[24]:

$$s \approx \frac{1-6kT}{W_m} \tag{13}$$

where, W_m is the binding energy or the maximum barrier height which has to be overcome by the carriers to transit from the long range mobility region to the short range mobility region. The binding energy (W_m) is calculated from the plot of $(1-s)$ versus T as shown in Figure 32 where the slopes of the straight lines are equal to $\frac{6k}{W_m}$. The as calculated values of the barrier height for the sample P0, PGE0.1, and PSE0.1 are included in the Table V. The values of the binding energy for the PGE and PSE composite films are less than the value obtained for the sample P0. This result support the lowering of the activation energy (E_a) for the composite films in comparison to the neat PVDF. Thus, it can be concluded that for the nanocomposites films, the field generated by the fillers results a decrease in the hopping barrier height and as a consequence the activation energy decreases. A closer observation to the Table V shows that the barrier height of the PSE composites is less than that of the PGE composites which is in accordance with the smaller value of activation energy for the PSE composite films in comparison to the PGE composite films.

Content Dependence of the ac Conductivity (σ_{ac}). Figure 33(a,b) depict the dependence of ac conductivity on the loading fraction of Er^{3+} ion at the frequency 100 Hz for the as synthesized PGE and PSE composite films, respectively. In Figure

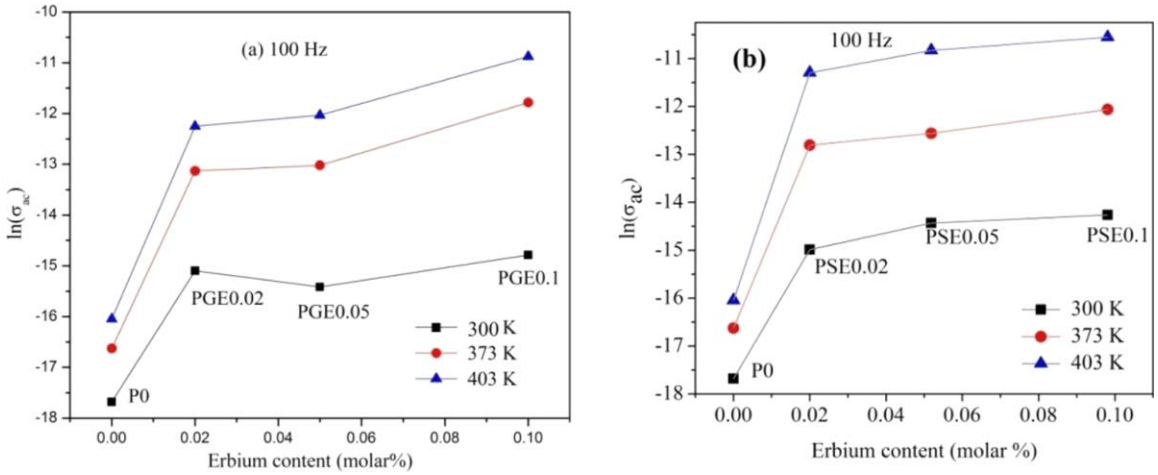

Figure 33. Variation of ac conductivity (σ_{ac}) at frequency 100 Hz with the loading concentration of Er^{3+} ion for (a) PGE composite films; (b) PSE composite films. [Color figure can be viewed in the online issue, which is available at wileyonlinelibrary.com.]

33(a), the variation of the ac conductivity for the PGE composite films shows a prominent increase in σ_{ac} value up to 0.02 molar % of erbium ion doping. After that, σ_{ac} becomes almost saturated for the higher loading fraction of erbium ions. The maximum values of ac conductivity at 300 and 403 K are obtained for the sample PGE0.1, which are found to be approximately 1.77×10^{-7} S/m and 1.88×10^{-5} S/m, respectively. A similar variation can also be observed for the PSE composite films with the maximum values obtained at temperatures 300 and 403 K as 5.3×10^{-7} and 1.06×10^{-5} S/m for the sample PSE0.1, respectively. This dissimilarity in the maximum value of the ac conductivity of the PGE and PSE films may be attributed to the interaction between the filler and the polymer matrix. The ac conductivity for PSE0.1 possesses a higher value in comparison to PGE0.1 at 300 K. On the other hand, at 403 K the ac conductivity for PGE0.1 is higher than that of PSE0.1. Thus, it can be concluded that $Er^{3+}@SiO_2$ has significant effect on the PVDF matrix at lower temperature whereas at higher temperature $Er^{3+}GeO_2$ plays the major role. This contrasting nature may be attributed to the less mobility of the large sized $Er^{3+}@GeO_2$ nanoparticles than that of the smaller sized $Er^{3+}@SiO_2$ nanoparticles.

CONCLUSIONS

A series of Er^{3+} ion doped GeO_2 and SiO_2 nanoparticles infused PVDF films were synthesized by a simple solution casting method. The mutually contrasting effect of the negatively charged nanoparticle surface and the positive Er^{3+} ions may take place in the PVDF matrix which retards the orientation of chain in TTT conformation. A lowering in the degree of crystallinity of the composite films with increasing filler loading is evident from the XRD results as well as DSC thermographs. This may be attributed to the increase in formation of complexes by the polymer chain around the Er^{3+} ions through cross linking mechanism. PSE composite films show higher value of dielectric constant than that of the PGE composite films at room temperature (300 K). However, at higher temperature the behavior is reversed due to the presence of larger sized low mobility complexes in PGE composite films. It can be inferred that at lower temperature the interfacial polarization is mostly responsible for the dielectric constant, but at higher temperature the immobilized polymer shells around the Er^{3+} ions play the key role for the enhancement of dielectric constant. The frequency variation of the tangent loss for the neat as well as composite films indicates the presence of the α_c relaxation process which is further confirmed by the frequency variation of the imaginary part of the dielectric modulus. Though the frequency variation of M'' reveals the existence of both the interfacial as well as α_c relaxation processes but for the composite films the α_c relaxation process is predominant. Thus, it can be concluded that the incorporation of $Er^{3+}@GeO_2$ and $Er^{3+}@SiO_2$ in PVDF mainly affects the crystalline region of the polymer matrix. Further an investigation on ac conductivity proves that the conduction mechanism for neat as well as composite PVDF films follows the Correlated Barrier Hopping model. As a whole, the loading of $Er^{3+}@GeO_2$ and $Er^{3+}@SiO_2$ nanoparticles in the PVDF matrix was found to significantly enhance the dielectric properties of PVDF without losing the flexibility of the composite films in a cost effective manner.

ACKNOWLEDGMENTS

One of the authors is thankful to INSPIRE, DST, Govt. of India (IF-140209) for providing partial financial support.

REFERENCES

1. El-Sayed, S. *Physica B* **2014**, *454*, 197.
2. Chafidz, A.; Kaavessina, M.; Zahrani, S. A.; Otaibi, M. N. A. *J. Polym. Res.* **2014**, *21*, 483.
3. Zhang, Q. M.; Bharti, V.; Zhao, X. *Science* **1998**, *280*, 2101.
4. Zhang, Q. M.; Li, H. F.; Poh, M.; Xu, H. S.; Cheng, Z. Y.; Xia, F.; Huang, C. *Nature* **2002**, *419*, 284.
5. Dang, Z. M.; Nan, C. W.; Xie, D.; Zhang, Y. H.; Tjong, S. C. *Appl. Phys. Lett.* **2004**, *85*, 97.
6. Martins, P.; Silva, M.; Lanceros-Mendez, S. *Nanoscale* **2015**, *7*, 9457.
7. Li, J. Y. *Phys. Rev. Lett.* **2003**, *90*, 217601.
8. Cheng, L. P.; Lin, D. J.; Shih, C. H.; Dwan, A. H.; Gryte, C. C. *J. Polym. Sci. Part B: Polym. Phys* **1999**, *37*, 2079.
9. Tawansi, A.; Oraby, A. H.; Ahmed, E.; Abdelrazek, E. M.; Abdelaziz, M. *J. Appl. Polym. Sci* **1998**, *70*, 1759.
10. Tawansi, A.; Ayad, M. I.; Abdelrazek, E. M. *J. Appl. Polym. Sci.* **1999**, *72*, 771.
11. Indra Devi, P.; Sivabharathy, M.; Ramachandran, K. *Optik* **2013**, *124*, 3872.
12. Zhang, S.; Wang, R.; Zhang, S.; Li, G.; Zhang, Y. *Chem. Eng. J.* **2013**, *230*, 260.
13. Martins, P.; Lopes, A. C.; Lanceros-Mendez, S. *Prog. Polym. Sci.* **2014**, *39*, 683.
14. Erdtman, E.; Satyanarayana, K. C.; Bolton, K. *Polymer* **2012**, *53*, 2919.
15. Satyanarayana, K. C.; Bolton, K. *Polymer* **2012**, *53*, 2927.
16. Thakur, P.; Kool, A.; Bagchi, B.; Das, S.; Nandy, P. *Appl. Clay Sci.* **2014**, *99*, 149.
17. Kar, E.; Bose, N.; Das, S.; Mukherjee, N.; Mukherjee, S. *Phys. Chem. Chem. Phys.* **2015**, *17*, 22784.
18. Takahashi, M.; Hara, Y.; Aoshima, K.; Kurihara, H.; Oshikawa, T.; Yamashita, M. *Tetrahedron Lett.* **2000**, *41*, 8485.
19. Silva, M. C.; de Camargo, A. S. S.; Silva, L. A.; Marletta, A. *J. Non-Cryst. Solids* **2008**, *354*, 5496.
20. Xie, F.; Zheng, Z. *Physica B* **2004**, *349*, 415.
21. Suzuki, H.; Hattori, Y.; Lizuka, T.; Yuzawa, K.; Matsumoto, N. *Thin Solid Films* **2003**, *438*, 288.
22. Huang, H.; Yan, B. *Mater. Sci. Eng. B* **2005**, *117*, 261.
23. Kumar, G. A. *Mater. Lett.* **2002**, *55*, 364.
24. EI-Sayed, S.; Abdel-Baset, T. A.; Hassen, A. *AIP Adv.* **2014**, *4*, 037114.

25. Hassen, A.; Hanafy, T.; Sayed, S. E. I.; Himanshu, A. *J. Appl. Phys.* **2011**, *110*, 114119.
26. Kepler, R. G.; Anderson, R. A. *Adv. Phys.* **1992**, *41*, 1.
27. Furukawa, T. *Phase Transit.* **1989**, *18*, 143.
28. Bose, N.; Basu, M.; Mukherjee, S. *Mater. Res. Bull.* **2012**, *47*, 1368.
29. Stöber, W.; Fink, A.; Bhon, E. *J. Colloid Interface Sci.* **1968**, *26*, 62.
30. Kochervinskii, V. V. *Russ. Chem. Rev.* **1996**, *65*, 865.
31. Dutta, B.; Kar, E.; Bose, N.; Mukherjee, S. *RSC Adv.* **2015**, *5*, 105422.
32. Abdelaziz, A. E. I.-K. M.; Hassan, G. M. *Int. J. Polym. Mater.* **2005**, *54*, 633.
33. Karthikeyan, P.; Suthanthirakumar, P.; Vijayakumar, R.; Marimuthu, K. *J. Mol. Struct.* **2015**, *1083*, 268.
34. Davis, E. A.; Mott, N. F. *Philos. Mag.* **1970**, *22*, 403.
35. Tawansi, A.; Oraby, A. H.; Zidan, H.; Dorgham, M. E. *Physica B* **1998**, *254*, 126.
36. Abdelrazek, E. M.; Holze, R. *Physica B* **2011**, *406*, 766.
37. Elashmawi, I. S.; Abdelrazek, E. M.; Ragab, H. M.; Hakeem, N. A. *Physica B* **2010**, *405*, 94.
38. Taha, A. *J. Appl. Phys.* **2012**, *112*, 034102.
39. Rekik, H.; Ghallabi, Z.; Royaud, I.; Arous, M.; Seytre, G.; Boiteux, G.; Kallel, A. *Compos. Part B* **2013**, *45*, 1199.
40. Lopes, A. C.; Costa, C. M.; Serra, R. S. I.; Neves, I. C.; Ribelles, J. L.; Lanceros-Mendez, S. *Solid State Ionics* **2013**, *235*, 42.
41. Silva, A. B.; Arjmand, M.; Sundararaj, U.; Bretas, R. E. S. *Polymer* **2014**, *55*, 226.
42. Pike, G. E. *Phys. Rev. B* **1972**, *6*, 1572.